SP-1272

CRYOSAT

SCIENCE REPORT

European Space Agency
Agence spatiale européenne

ESA SP-1272
March 2003

CryoSat Science Report

European Space Agency
Agence spatiale européenne

ESA SP-1272 – CryoSat Science Report

Report prepared by:	Mission Experts Division *Scientific Co-ordinator:* H. Rebhan *Scientific Editor:* M. Drinkwater Cryosat Project Team *Technical Co-ordinator:* G. Ratier
Cover:	Carel Haakman
Published by:	ESA Publications Division c/o ESTEC, Noordwijk, The Netherlands *Editor*: B. Battrick
Copyright:	© 2003 European Space Agency ISBN 92-9092-973-1 ISSN 0379-6566
Price:	€10

Foreword

This report describes the scientific rationale for the CryoSat mission together with the associated measurement requirements. It also provides information on the instrument concept and expected data products along with the requirements and plans for their validation.

The CryoSat mission is based on the mission proposal co-written and submitted in 1999 by a team of 18 scientific investigators led by Prof. Duncan Wingham, University College London, UK. The report compiles the current mission status from an extensive set of documentation that was prepared in conjunction with ESA's CryoSat Science Advisory Group during the development of the space and ground segments.

Further details, including the original documents, are publicly available from the CryoSat Web Site: www.esa.int/livingplanet/cryosat.

Contents

1 Introduction

1.1 The Earth Explorer Programme

In recent years the European Space Agency (ESA) has developed an overall strategy for Earth Observation for the time frame following the large observation platforms of ERS-1, ERS-2 and Envisat. This plan is based on a dual mission scenario which includes two complementary components, namely the Earth Explorer and Earth Watch missions.

The Earth Explorer missions have the fundamental aim of contributing to the provision of data essential to the study of the various Earth System processes, and to the extension of the existing hierarchy of models of the Earth System. They are also intended to help establish the feasibility of new space-based observation techniques of potential application in operational observing systems. The concept for Earth Explorers includes two lines of mission concepts.

The Core Missions will respond directly to specific areas of public and scientific concern and are selected through widespread consultation within the research and scientific communities. The development and implementation are ESA-led, with a new mission being launched approximately every two years.

The Opportunity Missions are tailored for more focused scientific applications with smaller satellites and a minimum set of observation instruments. This should allow a faster implementation schedule and a quicker response to evolving situations or areas of immediate environmental concern. The missions are initiated with an 'Announcement of Opportunity' (AO) addressing all scientific user communities. The AO solicits proposals which should describe in some detail a satellite and instrument concept for a particular scientific application. An essential element of this AO is an overall budgetary ceiling for the commitment of ESA. In introducing this concept, ESA posed European Earth scientists a question it had not done previously. It replaced the simpler question of what science desires, with the more difficult question of what science may be achieved within a fixed cost limit? The calls for Opportunity Mission proposals in 1998 and 2001 received an overwhelming response, demonstrating that scientists had plenty of innovative answers to this question.

1.2 The first call for Opportunity Missions

In October 1998 ESA issued the first Announcement of Opportunity for mission proposals from which the first Earth Explorer Opportunity Mission should be selected. More than 27 proposals were received and subjected to scientific review by different peer review groups with experts from different scientific areas. In parallel, a technical and programmatic assessment was performed. The results were summarised in an assessment report for each mission proposal. The Earth Science Advisory Committee (ESAC) was asked to list the proposed mission concepts in order of priority for implementation. CryoSat was endorsed as the first Opportunity Mission. This recommendation was subsequently approved by the Earth Observation Programme Board meeting in June 1999, which triggered two competitive feasibility and concept (Phase-A) studies. After the selection and consolidation of a single technical design concept, the mission was the subject of a second scientific peer review in 2000 that reconfirmed the feasibility and the importance of the scientific objectives of this mission. The concept and technical design for the space segment has been consolidated during the last 2 years and the major technical specifications are summarised in this report. The consolidation process did not compromise the original scientific arguments outlined in the proposal from 1999. We present these arguments together with the latest progress in cryospheric research in the following chapters.

2 Scientific Objectives

The cryosphere has a central role in the Earth's radiation budget. As a consequence of this feedback a loss of sea ice is predicted to cause a larger greenhouse-gas warming in the Arctic than the rest of the Earth. Ice sheets and glaciers together comprise one of the largest uncertainties in the potential sources of global sea-level rise. Variations in these components of the cryosphere can have a significant controlling influence upon sea-level variations. This chapter tries to emphasise and explain the major questions regarding the impact of the cryosphere on the Earth's climate and the benefits of specific altimetric observations.

2.1 The importance of the cryosphere

If we look at the role of the cryosphere for global climate phenomena, a large variety of time scales have to be considered. The Earth's Quaternary climate has been characterised on time scales of 100,000 years by interlinked changes in temperature, CO_2, ice sheets and sea level. More rapid global changes exposed in ice-core and other paleo climate records also appear to be related to fluctuations in the cryosphere (Bond et al. 1993). In contrast, interannual fluctuations in the modern climate reflect ocean-atmosphere interactions whose source is the tropical Pacific, but whose influence extends to the poles (Horel & Wallace 1981). Between these extremes lie fluctuations that we poorly understand and which operate on a great range of time scales. At the core of this uncertainty is our limited knowledge of the interactions of the cryosphere and atmosphere with the ocean thermohaline circulation.

In the modern climate, the ocean circulation is responsible for some half of the poleward heat transport, the remaining half being contributed by the atmosphere (Piexoto & Oort 1992). The release of heat from ocean to atmosphere in winter serves to maintain atmospheric temperature: mild winters in northwest Europe are a consequence. By the time warm water originating from the Gulf Stream has reached northern Europe and the Nordic Seas, the surface water has given up most of its heat to the atmosphere and becomes dense enough to sink in winter through deep convection. Surface waters are replaced by a fresher (and thus lighter) supply from the polar cryosphere. In some years these can form a fresh cap preventing deep convection (Aagaard 1994).

Trends in the supply of freshwater from the cryosphere may profoundly affect the thermohaline circulation, particularly in the North Atlantic region. Coupled models show a decline in the Northern Hemisphere poleward transport in response to increased freshwater supply (Manabe & Stouffer 1988), and/or greatly increased latitudinal variability (Weaver & Sarachik 1991). Such changes will have greatest impact on areas such as Europe that presently experience warm winter temperatures. The role of Arctic sea ice for the fresh water balance is of particular importance. Brine expulsion makes sea ice fresher than sea water. The wind-driven transport of sea-ice from the central

Arctic Ocean controls the freshwater budget of the Greenland Sea, the principal site of the overturning of the thermohaline circulation in the Northern Hemisphere. Therefore, variations in Arctic sea ice may have profound consequences for the poleward transport of heat by the North Atlantic.

2.2 Sea-level variations

On time scales of 10,000 years, fluctuation of ice sheets in the Northern and Southern Hemispheres has dominated variations in global sea-level. From 18,000 years ago, sea-level rose globally by 90 m as a result of the retreat of the Laurentide, Greenland and Scandinavian Ice Sheets (Peltier 1988). This rise in sea-level initiated, presumably, a shrinking of the marine Antarctic Ice Sheet, adding perhaps another 30 m to sea-level (Nakada & Lambeck 1988). This retreat appears to have been completed 5000 years ago. Since that time, sea-level appears to have been stable, varying by perhaps 10 cm, until the last century (Varekamp et al. 1992). Since then, according to more precise tide-gauge measurements, the rate appears to have accelerated, with a rise of ~15 cm over the past 100 years (Gornitz et al. 1982).

Changes in ice discharge generally involve response times of the order of 100 to 10,000 years. The time scales are determined by isostasy, the ratio of ice thickness to yearly mass turnover, processes affecting ice viscosity, and physical and thermal processes at the sea bed. Hence it is likely that the ice sheets are still adjusting to their past history, in particular the transition to inter-glacial conditions. Their future contribution to sea-level change therefore has a component resulting from past climate changes as well as one relating to present and future climate changes.

	Glaciers, ice caps	Greenland	Antarctic
Area (10^6 km^2)	0.68	1.71	12.37
Volume(10^6 km^3)	0.18 ±0.04	2.85	25.71
Sea-level-rise equivalent (m)	0.50 ±0.10	7.2	61.1
Accumulation (sea-level equivalent. mm/y)	1.9 ±0.3	1.4 ±0.1	5.1 ±0.2

Table 1. Physical characteristics of ice on Earth and their estimated contribution to global sea-level rise (Meier & Bahr 1996, Warrick et al. 1996, Reeh et al. 1999)

Nonetheless, the cryosphere is the largest potential source of sea-level fluctuations. It contains ~90% of the Earth's freshwater, largely in the Antarctic Ice Sheet. Together, the present Greenland and Antarctic ice sheets contain enough water to raise sea-level by almost 70 m, so that only a small fractional change in their volume would have a significant effect. The smallness of sea-level rise makes its explanation a challenge. The rate of 20th century rise is equivalent to the addition of 500 Gt/year of water. In comparison, the ocean annually exchanges 36100 Gt/year with the atmosphere, and

99000 Gt/year with the land (Piexoto & Oort 1992). The rise is therefore small, and may be explained by a number of competing geophysical processes, each of which is a complex process in its own right. These include tectonics; the redistribution of water from ice sheet and glacier retreat; the rebound of the lithosphere and mantle; the effect of these on the Earth's gravitational field; the thermal expansion of the ocean; the extraction of ground water; and changes in coastal sedimentation and erosion.

Some glaciologists (Thomas et al. 1979, Hughes 1981) have questioned the stability of the West Antarctic Ice Sheet, which contains sufficient water to change sea-level by 5 m. However, fluctuations of individual drainage basins are all that is needed to explain the 20th century rise, which corresponds to ~ 0.2% of Antarctic Ice Sheet mass. Little is known about fluctuations in ice sheets on this time-scale. The fast-flowing Antarctic ice streams, transporting ice from the interior, show a variety of dynamic behaviours, and evidence of change on century scales (Rignot 2002). Direct observations, variously interpreted, allow the imbalance of the Antarctic and Greenland Ice Sheets to explain all of the present rise, or none of it, or even a lowering sea-level (Warrick et al. 1996). Interferometric observations with Synthetic Aperture Radars (SARs) demonstrate rather strong dynamic changes for some ice streams in the West Antarctic ice sheet (Rignot 1998).

On the other hand, the fact that sea-level change appears to have accelerated in the last century points towards sources with faster time-constants than those associated with ice sheets. The 20th century sea-level rise is equivalent to 25% of the (estimated) mass of small ice caps and mountain glaciers. In this century, glacier retreat has been a notable feature of European and United States glaciers (e.g. Haeberli & Hoelzle 1995). The extension of observations of a few glaciers to those of the world at large is fraught with difficulty, but it appears that this may explain 4 cm of the present rise (Meier 1984). Thermal expansion of the ocean associated with global warming is also estimated to have contributed perhaps 4 cm this century (Cubash et al. 1992).

Thermal expansion and the melting of ice caps and glaciers are the largest expected sources of 21st century sea-level rise (Warrick et al. 1996). Changes for the next century due to global warming in Antarctica and Greenland are expected to be rather modest: -0.2 to 0.0 mm/y for Antarctica as result of increased precipitation and less than 0.1mm/y from Greenland from changes in both precipitation and runoff (IPCC 2001). In the longer term, the situation is different. Over 1000 years the Greenland Ice Sheet may contribute more than 2 m. Increased melting from the ice sheet is likely to drive its net surface balance close to zero (Wingham 1995). Iceberg calving will lower the altitude and surface melting will increase.

The prediction of future sea-level rise is therefore difficult. Estimates of the rise during the 21st century vary from 11 to 77 cm (IPCC 2001). This spans a range from modest coastline migration, to changes with profound political and economic consequences. It is essential that variations in the Earth's stores of freshwater are better determined than at present. As outlined earlier, the largest uncertainties are associated with the ice sheets, but all sources of sea-level rise are in urgent need of better definition. In addition to the impact of ice sheet variations, it is necessary to consider the effects of the global post-glacial rebound, possible changes in ground water reservoirs due to anthropogenic impact, and possible bias effects due to improved observing capabilities in the last century.

These questions involve small changes in mass over large areas of the Earth. Although in-situ observations may clarify the physics of the processes involved, satellites are the only method that can deliver data which may be used to constrain mass budgets on the large scale. Of these, ocean altimetry and time-variant gravity are very important.

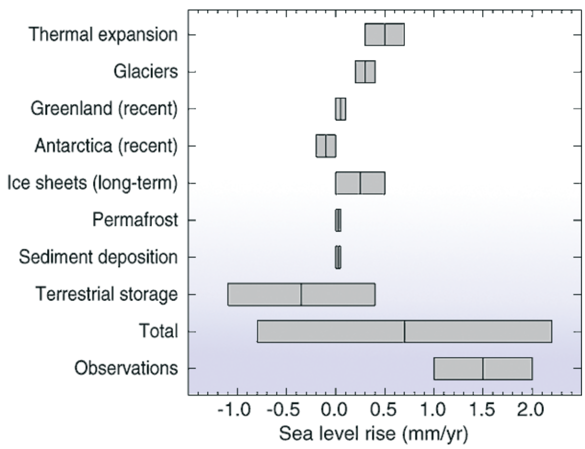

Figure 1. Ranges of uncertainty for the average rate of sea-level rise from 1910 to 1990 and the estimated contributions from different processes (IPCC 2001)

2.3 Ice sheet dynamics and mass imbalance

In-situ measurement of the imbalances of the Greenland and Antarctic Ice Sheets accounts for the snow accumulated at the surface and ice lost through surface ablation and ice flow over a grounding line (the line at which ice begins to float). This is difficult to accomplish accurately, partly because the grounding line fluxes are not well-known around the entire coastline. In the main, however, the error arises because the snowfall variability is difficult to sample properly. Glaciological estimates of Antarctic Ice Sheet mass imbalance (e.g. Bentley & Giovinetto 1991, Jacobs et al. 1992) vary from -500 to +500 Gt/yr (corresponding to ±1.4 mm/yr of sea-level change); similar estimates for Greenland range between -130 and +130 Gt/yr (Reeh 1991)

The estimated contribution of 0.4 mm/yr to 20th century sea-level change from ice caps and glaciers is equal to 8% of their mass. This is a substantial change. Only a small fraction of the Earth's glaciers and ice caps have their mass balance monitored. A global estimate extrapolates these estimates. Typically (e.g. Meier 1984) a correlation between observed surface balance, known for some glaciers, and for example snow accumulation, estimated more-or-less everywhere, is used to extrapolate the observations. There are two problems with this approach. Firstly, the correlation is often poor (e.g. Walters & Meier 1989). Secondly, the method ignores the calving flux. This is significant for many of the larger ice caps and glaciers in the Arctic and may bear no relation to surface balance. In short, this estimate should be treated with considerable caution. A greatly improved observational base is required.

Satellite observations have become a feasible method of determining the mass imbalance of the land ice fields in a timely fashion. The first attempt using the Seasat and Geosat altimeters (Zwally et al. 1989) predated the era of centimetre orbit accuracy and the reported elevation change has been questioned (Van der Veen 1993, Davis et al. 1998). The ERS satellites were the first to provide coverage of Antarctica and Greenland with centimetre orbit precision. In consequence, 63% of the Antarctic Ice Sheet (Fig. 2) is now known to be within 90 Gt/year (~0.25 mm/year of global sea-level rise) of mass balance. The mass imbalance this century is 60 ± 70 Gt/year or ~0.3 ± 0.4 mm/year of eustatic sea-level. Previous estimates of the grounded ice imbalance vary between -1.4 and +1.4 mm/year of sea-level rise. While demonstrating the great accuracy that satellite altimetry provides, 17% of the Ice Sheet margins, and 20% of the interior – together some 33% of the total land cryosphere – remain out of reach of the pulse-limited, ERS or Envisat radar altimeters. The chosen orbits for these satellites prevent observations in the interior. Furthermore, these altimeters are designed for the

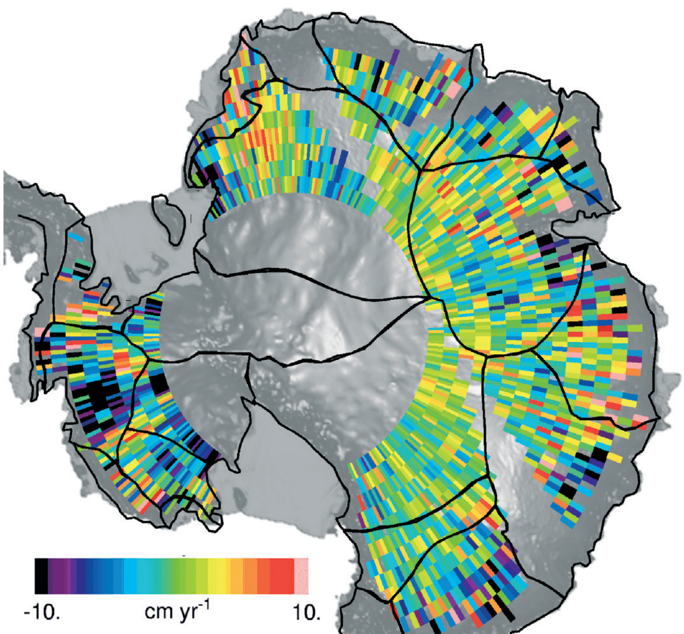

Figure 2. The change in elevation of the Antarctic Ice Sheet from 1992 to 1996 measured by the ERS-1 and ERS-2 altimeters (Wingham et al. 1998)

low-curvature surface of the ocean, causing the loss of returned signal in steeper terrains like ice sheet margins, ice caps and glaciers.

However, these areas could be critical for a better understanding of changes in the Arctic and Antarctic ice sheets. The margins are exposed to atmosphere and ocean forcing, are the most dynamic parts of the ice sheets (Alley & Whillans 1991), and may be undergoing change (e.g. Basin G-H in Fig. 2 is decreasing rapidly in elevation). The number of 17% for the non-observed area may appear a small proportion, but it accounts for 16% of the entire land cryosphere, and alone represents more than the entire Greenland Ice Sheet.

2.4 Sea ice dynamics and fluxes

Global ocean-atmosphere climate models are not yet able to reproduce observed sea ice extents in the Northern and Southern Hemispheres (Gates et al. 1995). Artificial flux corrections, which essentially hold the sea surface temperature to freezing in regions of climatological sea ice, put into question the calculation of the effect of "perturbations" such as CO_2-induced warming. The physics of sea ice in global coupled models is over-simplified. With the recognition that variations in thermohaline circulation may have important consequences for poleward heat transport, the next decade will see more complete sea ice physics within global ocean-atmosphere ice models.

On a regional scale, the evolution and verification of sea ice models has seen some significant progress in the last decade. The first ice models were pure thermodynamic models simulating the seasonal growth and decay of sea ice: i.e. Maykut & Untersteiner (1971), Semtner (1976), Lemke et al. (1990). One of the first dynamic-thermodynamic models was developed by Parkinson & Washington (1979). It was a 3-D model with four vertical layers: ocean mixed layer, ice layer, snow layer and atmospheric boundary layer. Free-drift ice dynamics was used. Hibler included the effect of internal ice stress, treating ice as a viscous, elastic, viscous-plastic (Hibler 1979) or elastic-plastic medium (Hibler 1986). An intermediate approach is the "cavitating fluid" approximation, which differs from free drift by allowing nonzero ice pressure under converging conditions, but, like free drift, offers no resistance to divergence or shear (Flato & Hibler, 1992).

The first coupled ice-ocean model was presented by Hibler & Bryan (1987), which coupled the Hibler ice model to the Bryan-Cox multi-level ocean model (Bryan 1969). This model, which is initialised by climatological temperature and salinity, shows that parts of the Barent and Greenland Seas are kept ice-free through the winter, but is less realistic with the ice thickness estimates.

Hakkinen & Mellor (1992) studied the large-scale variability of the Arctic ice using an 18-layer ocean model coupled to a 3-level snow-ice model. The viscous-plastic rheology scheme from Hibler (1979) has been used with other ocean models, i.e the

ECHAM/OPYC coupled model (Oberhuber 1992). An attempt at a more realistic coupled ocean sea ice model has been a coupling of the MICOM ocean model (Bleck et al. 1992) with a dynamic-thermodynamic sea ice model using Hibler's viscous-plastic rheology modified by Harder (1996). A favourable aspect of this model is the ability to provide high vertical resolution in regions of strong vertical density gradients and to suppress artificial numerical diffusion across isopycnals; both are important properties of the modelling of the Arctic Ocean.

With the introduction of more realistic sea ice models, it is obvious that observations will be needed to verify them. The lesson from regional sea ice modelling is that observed extents are of limited value in sea ice model verification. There are also essential differences in the parameterisation of certain important physical parameters. Regional models and global models may differ in terms of their specific thermal and albedo parameterisation of sea ice and snow. Differences between regional models are dominated by the parameterisation of sea ice rheology. Different rheologies may have different consequences for the longer term evolution of sea ice fields (Kreyscher 2000, Fig. 3) and yet are able to recreate the observed annual cycle of sea ice extent quite accurately (Ip et al. 1991, Flato & Hibler 1992, Fischer & Lemke 1991). There are essentially three different sea ice rheology schemes that are used for sea ice modelling today. The schemes are known as the viscous-plastic (VP), the cavitating fluid (CF), and the elastic-viscous-plastic (EVP) rheologies. The VP rheology dates back to the classical work of Hibler (1979), the most used cavitating fluid scheme is described by Flato & Hibler (1992), whereas the latest EVP rheology is discussed in a recent paper by Hunke & Dukowicz (1997).

What is needed to distinguish between rheologies are observations of sea ice thickness. In addition, in climate models, sea ice thickness provides a sensitive verification of the accuracy of atmospheric and ocean heat fluxes. These must be accurate to ~20 W/m^2 to achieve the correct thickness (Fischer & Lemke 1991). Presently, there are few direct heat flux or ice thickness measurements to compare with atmosphere-ocean-ice models at large spatial scales.

2.5 Primary and secondary mission goals

The scientific arguments for the importance of new cryospheric observations argued in the previous chapters determine the envisaged mission goals for CryoSat. The purpose of the mission is to determine trends in the ice masses of the Earth. Of principal importance is to test the prediction of thinning perennial Arctic sea ice due to global warming, and to reduce uncertainty in the estimated contribution to global sea-level rise of the Antarctic and Greenland Ice Sheets. These questions drive the primary mission goals. CryoSat will provide observations for:

- The determination of regional and basin-scale trends in perennial Arctic sea ice thickness and mass.

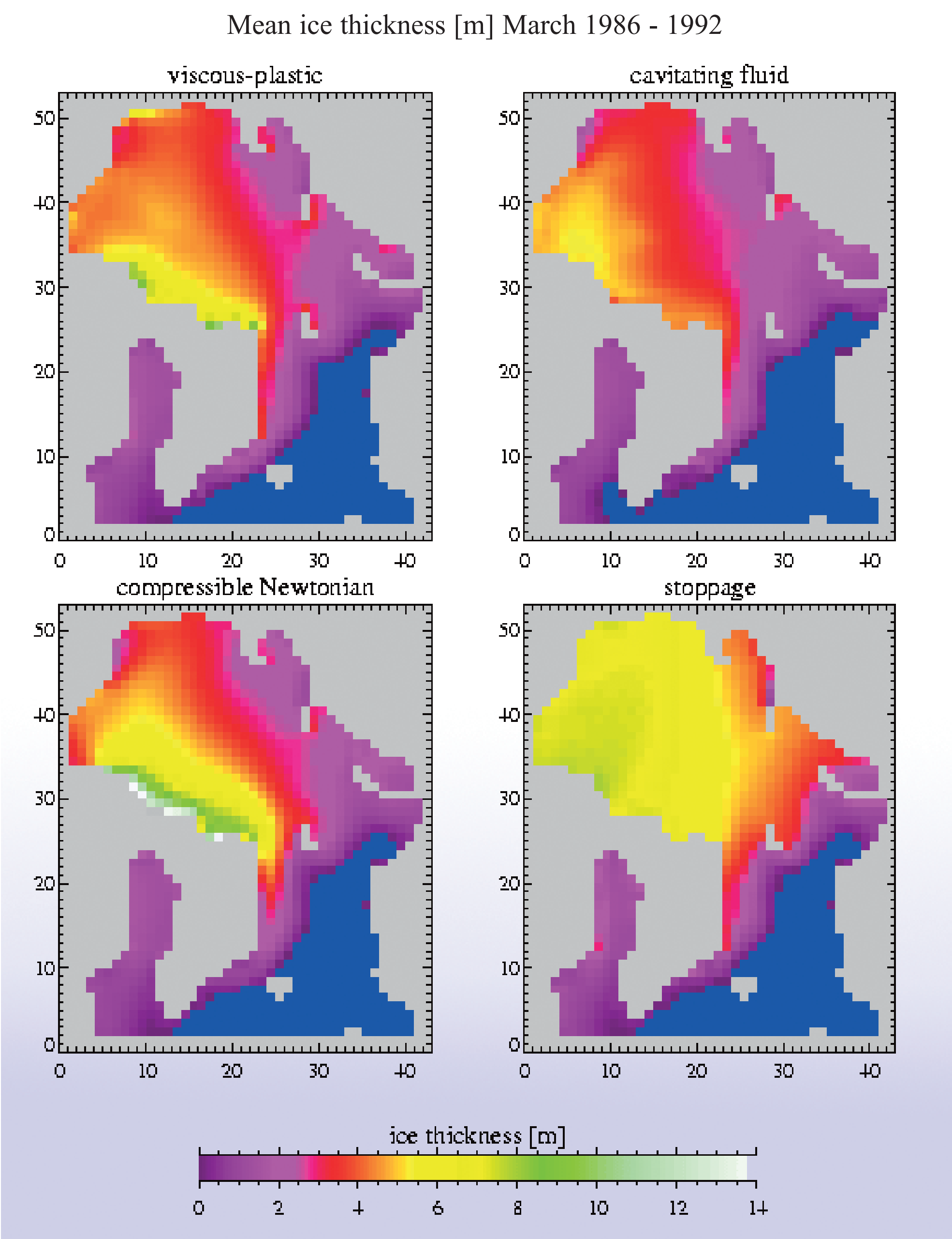

Figure 3. Comparison of sea ice models with different rheology (Kreyscher et al. 2000)

- The determination of regional and total contributions to global sea-level of the Antarctic and Greenland Ice Sheets.

Trends determined by CryoSat within its lifetime will be limited by the natural variability of ice thickness. The importance of its measurements will be increased by a future flight of an equivalent mission two decades or so later. Nonetheless, CryoSat will be able in its own lifetime to determine whether the observed changes in sea ice signal important long-term trends in Arctic climate, or merely reflect occasional variability at short spatial scales. In addition, CryoSat data will help to reduce the uncertainty in the ice sheet contribution to sea-level to a magnitude similar to that associated with other sources of sea-level rise.

CryoSat's secondary mission goals are to make observations of:

- The seasonal cycle and interannual variability of Arctic and Antarctic sea ice mass and thickness.
- The variation in thickness of the world's ice caps and glaciers.

These secondary goals have not been CryoSat design drivers. Nonetheless, CryoSat will make extensive measurements of seasonal sea ice fields and provide measurements over ice caps and glaciers, which has not been possible with previous altimeter systems. These measurements will effectively complement remote sensing data from other satellite missions, which have been used for cryosphere observations in the last decades.

2.6 Current remote sensing capabilities

In order to demonstrate the uniqueness and complementary character of CryoSat observations, the current status of remote sensing in the polar regions needs to be reviewed.

Sea ice extent and concentration (i.e. percentage coverage of the water surface) has been easily and continuously observed by passive microwave sensors on satellites since 1973.

The satellite data most commonly used for comparison with sea ice models are passive microwave data (SMMR and SSM/I data), which give regular temporal and spatial coverage of all ice areas. The spatial resolution, which is of order 30 km, is ideal for use with ice-ocean models which have similar or coarser resolution. The passive microwave data provide over 20 years of ice area and ice concentration observations in both hemispheres. This is in fact one of the most comprehensive remote sensing data sets used for geophysical research. The data sets are primarily used to validate the performance of large-scale and regional models in simulating the seasonal and interannual variability in ice area and extent. AVHRR and other optical/IR data have been used by the operational ice services for many years together with SSM/I data to produce ice charts. These ice charts are also used to validate ice models. Preller et al. (1992) provided an extensive review of the use of satellite data in ice models.

Another notable result from passive microwave instruments has been the long-term observation of the Weddell Sea Polynya from 1973 to 1976 and the recognition of the enormous heat losses from the ocean that may occur as a result (Gordon & Comiso

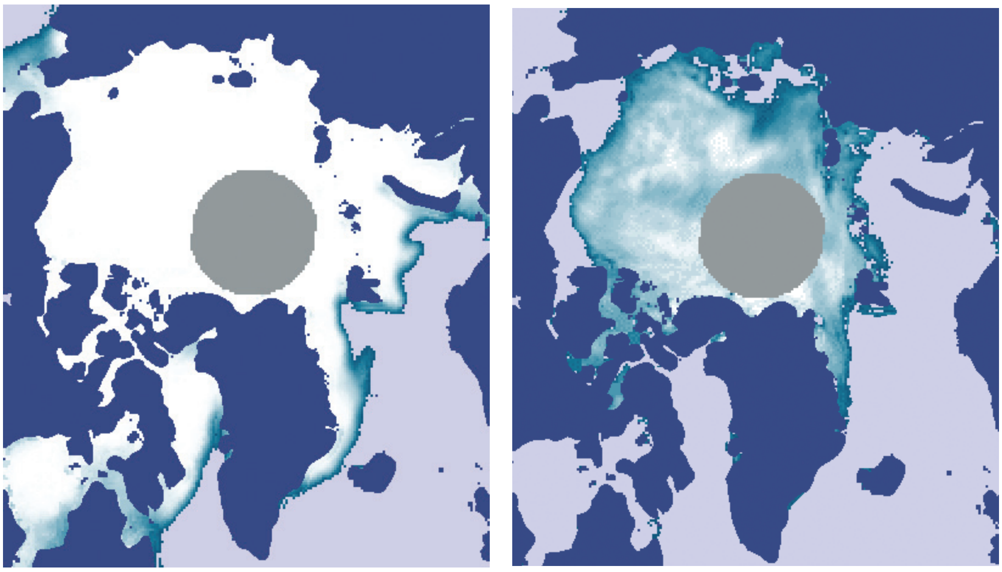

Figure 4. Examples of monthly mean total (left) and multiyear fraction (right) ice concentrations for December 1980 in the Northern Hemisphere. White: 100 %; Blue: < 15 %. Open water is light purple

1988). Even more important was the first evidence from remote sensing data that Arctic sea ice cover as a whole may be shrinking (Johannessen et al. 1995, Cavalieri et al. 1997).

Analysis of the 20 year time series of global ice data shows that the Arctic ice area has been reduced by 0.3×10^6 km^2 per decade (Fig. 5), corresponding to ~3% of the ice area (Bjørgo et al. 1997). The hemispheric ice covers fluctuate quasi-periodically, with predominant periods of between 3-5 years, though their variability is apparently not correlated. Regionally, the trends vary significantly. The most pronounced reduction is found in the Kara and Barents Sea, with more than a 10% decrease in ice extent per decade, while ice areas off eastern Canada show an increasing trend (Parkinson et al. 1999).

Sea ice velocity, previously known only from drifting buoy measurements, has been determined through repeated passive microwave and scatterometer observations and with greater spatial resolution with repeated Synthetic Aperture Radar (SAR) measurements (Kwok et al. 1990).

2.7 Sea ice thickness estimates with Altimetry

Freeboard measurement using satellites is the only technique by which to estimate sea ice thickness with the time and length scales that investigation of the Earth's climate demands. Observation strategies were discussed already 20 years ago (Robin et al. 1983) and a first analysis of altimeter waveforms reflected from sea-ice was done with airborne measurements, Seasat, and Geosat altimeter data (Fetterer et al. 1992). However, it was the Radar Altimeters (RA) of ERS-1 and 2 that allowed for the first

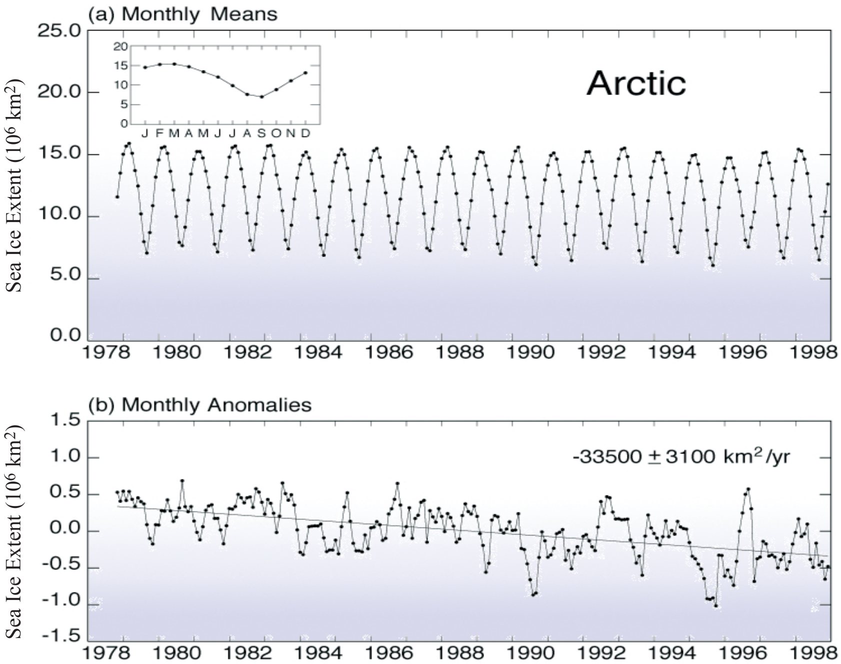

Figure 5. Time series of sea ice area measurements in the Arctic as observed from satellites from 1978 to present, after removal of the seasonal variability (Zwally et al. 2002)

time a more comprehensive analysis to estimate sea ice thickness trends for the whole Arctic basin. Being optimised to operate over the oceans, the ERS sea ice observations are limited by the resolution of the altimeters, a situation that will continue with Envisat and Jason-1.

The first step in generating estimates of ice freeboard is assessment of the (unobserved) sea surface elevation using elevation estimates from several orbits. In the case of ERS RA observations, the satellite passes over the same ground track every 35 days, permitting the analysis of cross-over orbits to estimate a mean sea-level. Co-located elevation estimates identified as open water/thin ice are time-averaged at each point of the ground track to obtain mean and variance for sea surface elevation. The mean profile is then subtracted from individual profiles to obtain a residual. The elevation of the water surface beneath the ice floe is then determined using linear interpolation of the sea surface residual on either side of the ice returns (Fig. 6).

A first attempt to exploit this technique and to derive a time series for average sea ice thickness distributions in the Arctic has been made by Laxon et al. (2001). By collecting all available ERS altimeter data from the years 1993-99 a simple linear regression of ice thickness estimates could be made for a series of grid points covering the Arctic Ocean. Figure 7 shows the results in comparison with locations of corresponding sub-marine data from the SCICEX cruises overlaid. The overall trend of -1.1 cm/year is in close agreement with trends observed by Johannessen (1999) using

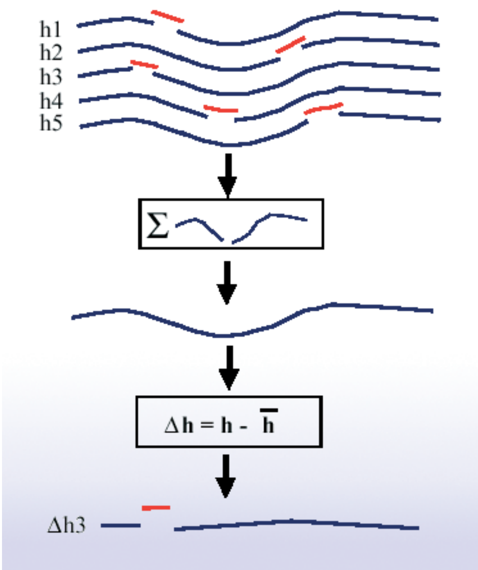

Figure 6. Ice freeboard estimation through co-linear analysis. Specular returns (blue) are used to generate a mean sea surface, which is then removed from individual passes. The elevation difference between diffuse (red) echoes and residual sea surface height is then used to estimate ice freeboard. Currently up to 60 profiles are averaged to obtain a mean sea surface (Laxon et al. 2001)

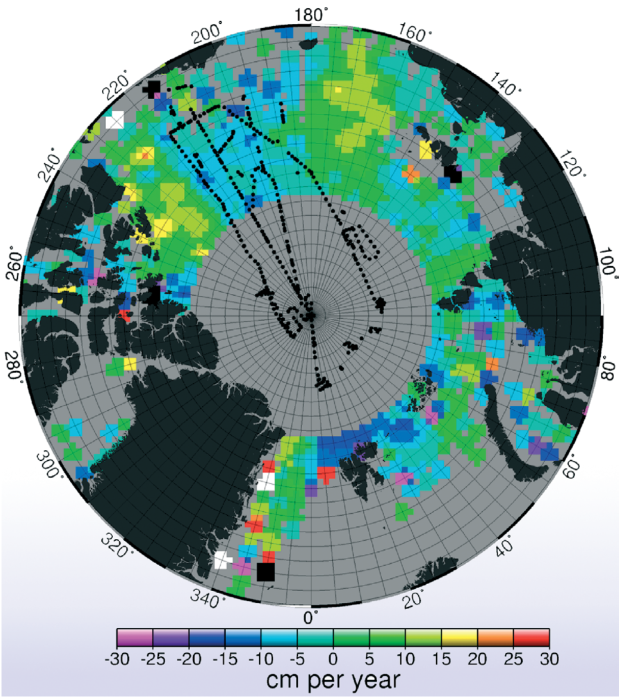

Figure 7. Trends in Arctic ice thickness 1993-1999 from ERS-1/2 altimeters (Laxon et al. 2001)

Russian data sources, but is significantly less than that observed in the submarine data analysed by Rothrock et al. (1999).

The results are promising and demonstrate the potential of altimetric observation for sea ice thickness estimates. However, they also highlight the specific deficiencies of a conventional pulse-limited altimetry system. The retrieval technique requires sufficient samples from ice and open water observations to obtain a realistic statistical analysis. The distinctive waveforms from ice reflections for a conventional altimeter limit the ability to separate ice from water. A clear distinction of the ice is possible with an average of only 5% of the observations. The presence of sea ice within the radar altimeter footprint generally changes both the shape and power of the return echo received. These changes are attributable both to reflections from sea ice itself and to changes in the water surface caused by the presence of ice. Radar altimeter echoes over sea ice fall into one of three categories: (i) Specular, (ii) Diffuse or (iii) Complex (Fig. 8). Specular echoes make up between 50-80% of the return echoes observed in current pulse limited space-borne altimeters.

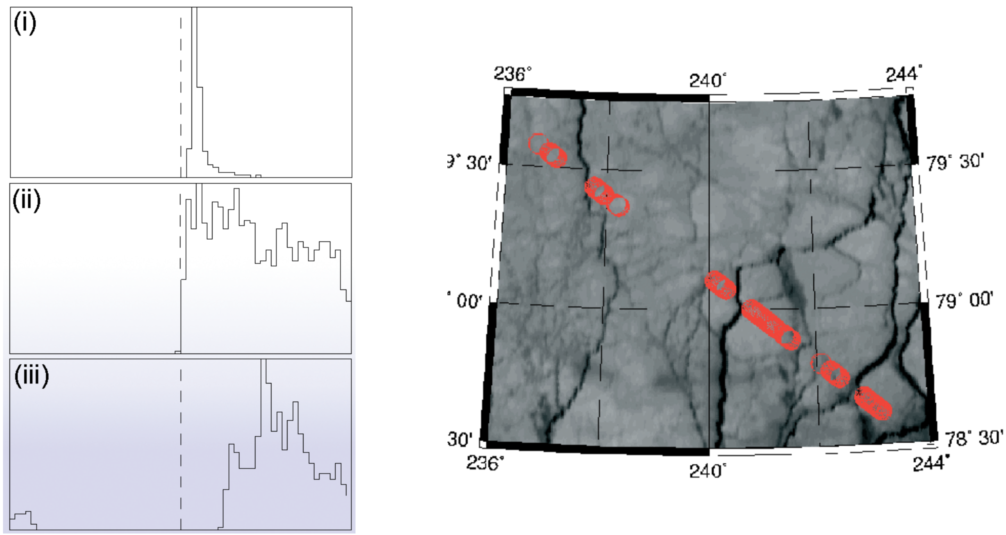

Figure 8. Radar altimeter echo types observed over sea ice. Specular returns (i) originate from leads and thin new ice, while complex echoes (ii) originate from the surface of ice floes. Complex echoes occur when a heterogeneous mixture of ice and water occurs within the altimeter footprint and are discarded because an unambiguous elevation cannot be retrieved. This is illustrated on the right where ERS altimeter footprints are overlaid on AVHRR imagery. Diffuse echoes are only observed where consolidated ice cover fills the altimeter footprint. Specular echoes occur over visible and sub-pixel lead. Data gaps indicate the location of complex echoes. (Laxon et al. 2001)

Specular echoes are characterised by a rapid fall off in return power after the initial rise indicating a highly specular reflecting surface, and in addition the peak power can exceed that typically observed over the open ocean by up the three orders of magnitude (30 dB). The origin of these specular echoes is not fully understood, but consideration of normal incidence backscatter theory and some assumptions regarding the amount of perfectly flat ice and water reflectors offer some clues as to their likely origin (Robin et al. 1983). Firstly, the generation of echoes that fall off within the narrow range of incidence angles sampled by the altimeter implies that the reflecting surface must be flat or smooth to within a fraction of the wavelength (say l/8 = 3 mm) over distances of several metres. Secondly, reflections from such surfaces can, theoretically, dominate the altimeter echo even if they represent less than 1% of the reflecting area within the altimeter footprint. Although mm scale measurements of sea ice roughness are scarce, those that do exist indicate that specular echoes are unlikely to originate from (first- and multi-year) ice floes and can only originate from areas of open water or new ice within the pack. This hypothesis is supported by measurements of normal incidence backscatter from ice and water surfaces. Experiments on artificial sea ice show that backscatter from a calm water surface can exceed that from rough ice by 20 dB (Gogineni et al. 1990). Measurements of the radar backscatter at 13 GHz from aircraft in the early 1970's show the strongest returns at nadir (σ_0=15 dB) originating from open water within the pack ice, with backscatter decreasing from 6 to 0 dB as the ice thickness increased from 5 to 360 cm (Parashar et al. 1974). By isolating specular echoes, therefore, it is possible to accurately retrieve estimates of the instantaneous sea surface elevation even in areas of high ice concentration. This has, for example, enabled the derivation of high resolution marine gravity fields in ice infested waters (McAdoo & Laxon 1997).

Diffuse echoes, such as those typically observed over the open ocean, are less common in areas of high ice concentration, making up only 5% of returns during the winter and virtually none during high summer.

These limitations demonstrate the need for a higher resolution altimeter to ensure a proper sampling of sea ice for flux estimations in the Arctic Basin. In the following chapter, the exploitation of synthetic aperture processing for the CryoSat altimeter to compensate for these limitations is demonstrated.

3 The Instrument Concept

The primary payload for CryoSat is a radar altimeter with extended capabilities to meet the observation requirements for ice sheet elevation and sea ice freeboard estimates. The remaining components on the instrument platform are for a highly accurate orbit determination and precise attitude control. This includes the DORIS system, a laser reflector and star trackers.

3.1 The SIRAL altimeter

CryoSat will provide an altimeter system for the ice sheet interiors, for sea ice and for ice sheet margins and other topography. Technically it is based on the Poseidon Altimeter developed for the French-US Topex/Poseidon mission. The new operations modes are based on the developments in Europe and the USA (Phalippou 1998, Raney 1995). A first airborne demonstrator has been build at Johns Hopkins University in Maryland (Raney 1998), a European version is under construction (Mavcrocordatos, personal communication).

Three operating modes are foreseen:

- Conventional pulse-limited operation for the ice sheet interiors (and ocean if desired).
- Synthetic aperture (SAR) operation for sea ice.
- Dual-channel synthetic aperture/interferometric (SARIn) operation for ice sheet margins

The principal objective of a satellite radar altimeter is to measure the time delay in receiving reflected signals from ground facets scanned by passage of the instrument overhead. Geophysical elevation is derived from the record of radar height measurements, corrected with respect to precise orbit knowledge and path delays. Height precision is set by the radar pulse length and by the amount of averaging available for each estimate. Height is defined as the minimum range between the radar and scatterers that lie along the ground track of the satellite.

A conventional satellite altimeter uses the echo delays from within the pulse-limited footprint to estimate minimum radar range. Outside the pulse-limited footprint, each scatterer echo appears with relatively greater delay. The pulse length determines the diameter of the pulse-limited footprint associated with a corresponding area on the ground. For a typical radar altimeter, such as GEOSAT, the pulse-limited footprint is in the order of 2 km in diameter, expanding to many kilometres as large-scale surface roughness increases.

The new *Synthetic Aperture* mode will allow more efficient operation. This is achieved by compensating for the systematic range delay errors; thus, the entire (beam-limited) along-track signal history contributes to height measurement, rather than only the much smaller pulse-limited area. In other words, the altimeter uses much more of the instrument's radiated energy than a conventional beam-limited altimeter.

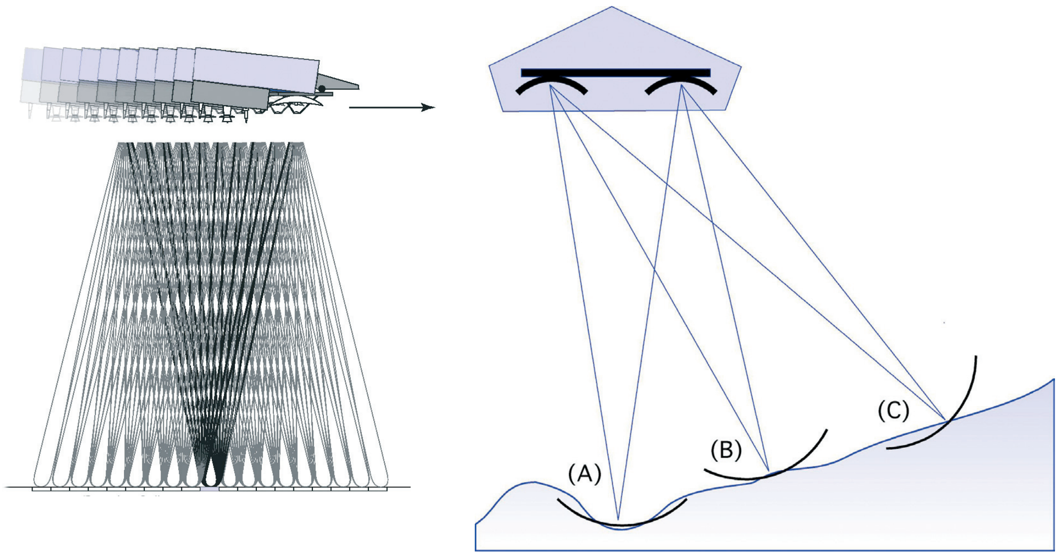

Figure 9. Principal operating modes of the SIRAL altimeter. Left: SAR-mode over sea ice. Right: SARIn-mode over steep ice sheet terrain

The synthetic aperture processing will be applied over sea ice for enhanced resolution along track. Over a spherical surface, the range rings of the pulse-limited altimeter are divided by the Doppler beams into range slices falling across the track (Fig. 9 left, 10 beams are shown only for clarity). The resolution over a plane surface is the stippled region of the footprint. The footprints of different sub-beams over a flat surface are adjacent rectangular areas ~250m wide along track and as large as the antenna footprint across track with up to 15 km width. The individual Doppler beams are collected ('stacked') together for all beams pointing towards a particular strip on the surface.

The *SAR-Interferometric* mode of SIRAL is intended to provide improved elevation estimates over ice sheets with variable topography. Generally, over ice sheets the surface is not plane, and a method for determining the echo location is required. A second synthetic aperture system is added and used to form an interferometer across the satellite track. The angle of the echo at each range may be determined, and this, together with the range, determines the elevation and across-track location of the surface. The 64 echoes are phase multi-looked to reduce speckle, and to estimate the coherence at each range. When the across-track echo direction in (Fig. 9 right) is unambiguous, as in (a) or (c), its coherence is high. Echoes at ranges with ambiguous directions, because two or more points on the surface have the same across-track range, as in (b), have low coherence, and may be masked. The data rate is about twice as high as for the SAR mode. In order to cope with abrupt height variations, the range-tracking concept for this mode has to be particularly robust. In SIRAL, this is ensured by using narrow-band tracking pulses, transmitted in-between successive wide-band measurement bursts.

Instrument mode	Pulse limited	SAR	SARIn
Receive chain	1	1	2
Samples per echo	128	60 m	512
Range window	60 m	60 m	240 m
Bandwidth	350 MHz	350 MHz	350 MHz
PRF	1970 Hz	17.8 kHz	17.8 kHz
TX pulse length	51 ms	51 ms	51 ms
Useful echo length	44.8 µs	44.8 µs	44.8 µs
Burst length	-	3.6 ms	3.6 ms
Pulses per burst	-	64	64
Burst repetition interval	-	11.7 ms	46.7 ms
Azimuth looks (46.7 ms)	92	240	60
Tracking pulse bandwidth	350 MHz	350 MHz	350 MHz
Samples per tracking echo	128	128	128
Size of tracking window	60 m	60 m	480 m
Average tracking pulses (46.7 ms)	92	32	24
Data rate	51 kbps	12 Mbps	2 × 12 Mbps
Power consumption	100 W	135 W	130 W

Table 2. Key instrument parameters of SIRAL

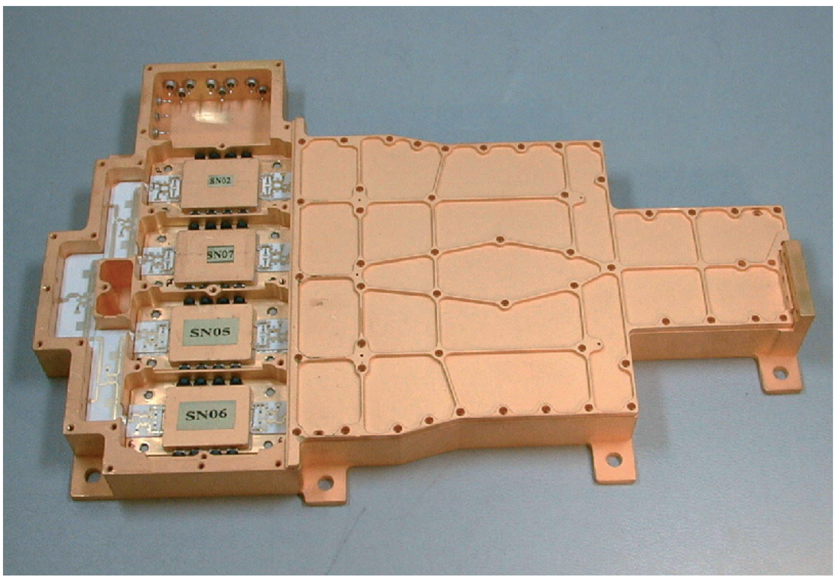

Figure 10. Breadboard model of the solid-state power amplifier for the SIRAL altimeter. It consists of four identical amplifier modules and a waveguide structure

3.2 DORIS

DORIS is an up-link radio-frequency tracking system based on the Doppler principle, which is operational on several satellites in orbit and in development. It is supported by a ground network of in excess of 50 beacons. Every 10 seconds the receiver on-board measures the Doppler shift of the signals continuously transmitted from the ground beacons at the two frequencies of 2036.25 MHz and 401.25 MHz. The on-board ultra-stable oscillator provides the reference for this measurement with a stability of 5×10^{-13} over 10 to 100 seconds.

In CryoSat's case the following DORIS services will be used:

- on-board:
  - real-time orbit determination for satellite attitude and orbit control;
  - provision of the SIRAL instrument with a precise 10 MHz reference signal;
  - provision of a precise time reference based on international atomic time (TAI);
- after storage and downlinking, on the ground:
  - provision of precise obit determination;
  - provision of ionospheric modelling.

Figure 11. Essential parts for the CryoSat space segment: Star Tracker with optics and baffle (left) and DORIS antenna (right)

3.3 Star Tracker

The Star Tracker is the principal means of determining the orientation of the SIRAL interferometric baseline. It is also the principal 3-axis attitude measurement sensor in the nominal operating mode. It is a lightweight, low power consuming, fully autonomous device capable of delivering high-accuracy inertial attitude measurements in order to satisfy the high pointing knowledge requirement of CryoSat. A set of three autonomous Star Trackers will be accommodated such that the Sun and Moon can each blind only one head at any time. This multiple configuration makes the sensor system one-failure tolerant, except for the rare occurrence of simultaneous Sun and Moon blinding of two heads, to which the system software is tolerant. Consequently, two camera heads are operated in parallel at full speed at all times. All three Star Trackers are mounted on the space-exposed payload antenna bench of the CryoSat satellite in order to optimise the structural stability between the star sensors and the antennas frame.

3.4 Laser Retro-Reflector

The Laser Retro-Reflector (LRR) is a passive optical device for precise ground-based measurement of the satellite orbit. Such devices have been used on several European, American and Russian satellites. The CryoSat LRR will be based on an existing LRR design. It will be accommodated on the nadir plate of the satellite with good visibility to Earth to allow operation at elevation angles above 20° for all azimuths. In view of the high measurement precision, the LRR will be accommodated as close as possible to the satellite COG to avoid any measurement inaccuracies caused by satellite motion.

4 Observing Capability

4.1 Definition of requirements

The CryoSat mission will determine trends in ice mass through repeated measurements of ice thickness (h) . Due to the limited mission duration, a residual uncertainty in the mass and thickness trends of sea and land ice will remain at the end. The scientific requirements are determined by this residual uncertainty. It should be recognised that it cannot be smaller than the natural variability in thickness. There is limited value in making observations with greater precision than the natural lower limit. The determination of requirements is thus a two-stage process. The first task is to characterise the natural variability of thickness. The second is to determine the measurement accuracy that makes the residual uncertainty close to the natural variability. This is the required measurement accuracy. These considerations lead to the science and measurement requirements in Table 3. The aspect of natural variability is addressed in more detail in the chapter on data validation.

With the parameter h we describe ice thickness when referring to sea ice, and ice elevation when referring to land ice. The principal goal, however, is to derive changes in mass rates and fluxes. The notation η is used to describe variability of a mass rate, quoted typically in units of Gt/year. This is useful to compare a mass variation with sea-level rise (1 mm/year eustatic sea-level equals 360 Gt/year of water). The symbol σ is used to describe the variability of a mass rate per unit area. This is a more convenient quantity to compare with a change in thickness ($\delta h/\delta t$), and for this reason σ is noted as cm of ice mass/year, assuming a density of 915 kg m^{-3}, written cm/year ice equivalent (i.e.). In general a good deal of the variability in ice mass occurs at short spatial scales, and the variability of mass is a strong function of the area under consideration. The symbol $\overline{\sigma} = \eta/A$ characterises the mass variability of an extensive area A as a thickness variability. If the mass variation is perfectly correlated over an area A, then $\overline{\sigma} = \sigma$, but this is generally not the case. Typically $\overline{\sigma}$ will be considerably smaller than σ for areas in excess of 10^4 km^2.

The scientific requirements specify the residual uncertainty $\overline{\sigma}_r$ in trends at the end of the mission. The lowest bound of the residual uncertainty is the natural variability $\overline{\sigma}_n$. Measurement error $\overline{\sigma}_m$ will increase residual uncertainty according to

$$\overline{\sigma}_r^2 = \overline{\sigma}_n^2 + \overline{\sigma}_m^2 \qquad (1)$$

The residual uncertainty is determined by requiring it to be close to the natural lower bound, and we give close a quantitative expression by requiring that the observations increase by no more than 10% the residual uncertainty in a trend due to natural variability, i.e.

$$\overline{\sigma}_r = 1.1\overline{\sigma}_n \qquad (2)$$

The variation of $\overline{\sigma}$ that results for ice sheets is illustrated in Figure 12 as a function of spatial scale.

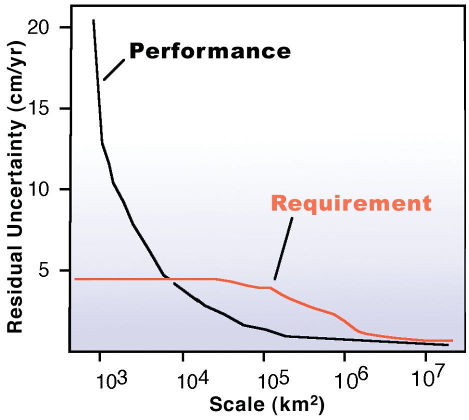

Figure 12. Comparison of the required and actual accuracies of ice sheet imbalance measurements by CryoSat. To meet the requirements across the range of horizontal scales from 10^4 km^2 to 10^7 km^2, the actual accuracy is smaller than need be at large scales

The measurement requirements are then determined by substituting Equation (1) into Equation (2) to obtain

$$\overline{\sigma}_m = 0.5\overline{\sigma}_n \qquad (3)$$

It is not practical with a single satellite to satisfy Equation (3) at all of the spatial scales. The actual measurement error will become large at small spatial scales, as the figure shows. Therefore it requires that Equation (3) be satisfied over a narrower range of scales. In the case of sea ice, a typical areal extend of 10^5 km^2 can be considered as the lowest scale at which trends may become visible. In the case of the ice sheets, there are important scientific questions at regional and continental scales. Equation 3 needs to be satisfied at 10^4 km^2 *and* at 14×10^6 km^2. The latter is the total area of the Ice Sheets (comp. with Table 1). This leads to the requirements shown in Table 3.

Requirement [cm/year]	Arctic Sea Ice 10^5 km^2	Ice Sheets 10^4 km^2	Ice Sheets 14×10^6 km^2
$\overline{\sigma}_r(\eta_r)$ i.e	3.5	8.3	1.0 (130 Gt yr $^{-1}$)
$\overline{\sigma}_m$	1.6	3.3	0.7

Table 3. The CryoSat science and measurement requirements

4.2 Orbit selection

As with every altimetry satellite, the selection of the orbit is a major driver for the observing capability. For ice sheet observations, a maximum number of cross-over track points are desirable to maximise the number of retrievals for a certain location. However, for drifting sea ice the repeated observation of a fixed location is not necessary. For these measurements, the goal is to maximise the number of tracks for a certain area (see Section 2.7). The wish for complete coverage of the polar caps with a true polar orbit (inclination = 90°) would be compromised by loss in cross-over tracks and technical constraints. However, there is no need for a Sun-synchronous orbit, which allows more flexibility in the orbit selection. The nominal orbit of CryoSat, called the Science Orbit, has been defined to provide a compromise between good coverage at higher latitudes and a maximum number of cross-over points (Table 4). The major parameter for this optimisation is the orbital inclination. The variation in the number of cross-overs per 100 km^2 for a 1-year repeat orbit, at inclinations of 92°, 93° and 94°, for a latitude range of 60° to 90°, is shown in Figure 13. Clearly, then, the selected inclination of 92° is a compromise between reducing the loss of sea ice coverage at the North Pole, and maintaining the measurement requirement in southern Greenland.

	Altitude	Inclination	Repeat	Eccentricity
Science Orbit	717,242 km	92°	369 days (30 day sub cycle)	0.0014 (near circular)
Validation Orbit	711,346 km	90°	2 days	

Table 4. Orbital parameters for CryoSat

In order to support the calibration and validation activities during the Commissioning Phase, a dedicated validation orbit has been defined which provides a short 2-day repeat cycle. Field campaigns in polar regions should be complemented with a maximum number of simultaneous CryoSat measurements. The satellite will stay only one month in this orbit before being transferred to the nominal Science Orbit.

4.3 Instrument simulations

Whereas there is much experience with conventional pulse-limited altimeter systems like ERS-RA or Topex/Poseidon, an instrument like SIRAL with SAR processing has never been flown in space. This requires numerical simulations of the expected performance in SAR and SARIn mode. With the original CryoSat proposal only very premature simulations were available and so several new analyses have been conducted

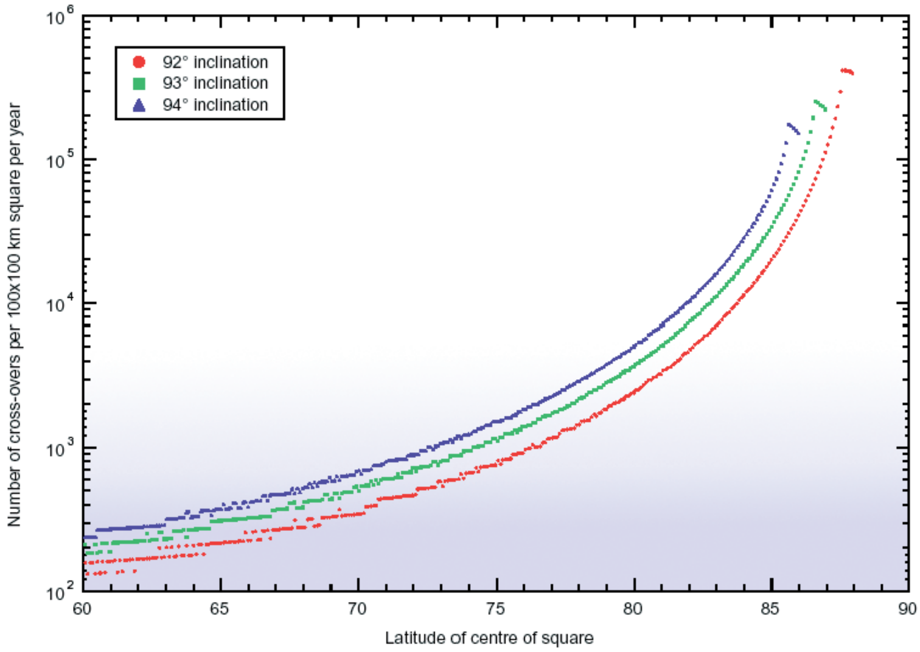

Figure 13. CryoSat orbit selection: The variations in the number of cross-overs per 10 km^4 for a 369-day repeat for a latitude range of 60° to 90°

with more realistic assumptions about the envisaged target areas of sea ice and ice sheets.

4.3.1 Synthetic aperture measurements for sea ice

For a first estimate of the expected performance, the expected altimetric waveforms needed to be simulated with some realistic assumption about the distribution of ice and water within the instrument footprint. Using a simplified, first-stage instrument simulator for CryoSat, this simulation study was conducted by Laxon et al. (2001). Typical two-dimensional distributions of ice and water have been obtained from optical imagery taken by US satellites (Fig. 14). Elevations have been derived from submarine draft statistics (SCICEX cruises) and typical values for radar backscatter have been based on observations with ERS altimeters. Synthetic observations of sea ice have been generated using a number of mission scenarios combined with models describing the statistical and surface properties of sea ice which may affect the quality of the observations. The ultimate aim was to provide a first-order statistic on the instrument's performance for different ice/water mixtures and a variation in overall ice concentration. The generation of an instrument surface model required several steps. First a floe geometry model was constructed from the optical imagery describing the horizontal distribution of ice and water within the instrument field of view. These geometry models were then superimposed with a realistic vertical topography based on a given mean snow and ice thickness. Finally, it was necessary to attribute backscatter

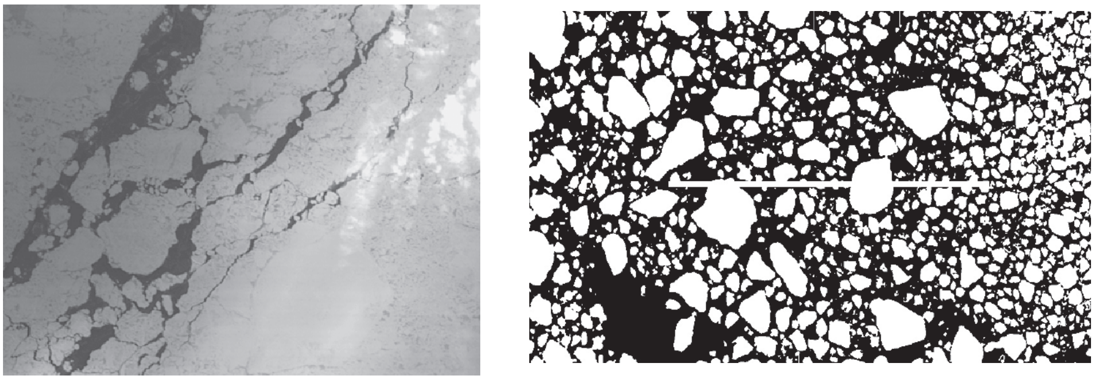

Figure 14. High resolution optical images of the Beaufort Sea from a US reconnaissance satellite (left) and an airborne mapper (right) from the MIZEX campaign. These images were used to derive the floe geometry models for the altimeter simulations (Laxon et al. 2001)

characteristics to the ice and water surfaces within the footprint, depending on realistic assumptions of snow cover and the state of surface melt.

For each of these instrument surface models, the simulator generated estimates of surface elevations along with a mean power echo calculated from stacked waveforms of the complex echoes. The stacked waveforms were retracked using a simple 50% threshold retracker as described by Laxon & McAdoo (1994) to obtain more accurate estimates of sea surface height. The bin width of the resulting waveforms corresponds to an elevation of 45.3 cm, with a fine waveform shift of 7.1 mm, which essentially defines the vertical resolution of the simulator. In order to distinguish between retrievals from open water and those from ice, a simple thresholding algorithm was applied to the peak power. From experiments with the simulator output from an ISM containing both flat ice and water, waveforms with a peak power greater than -110dB were considered to originate from open water with backscatter set to 40 dB. For open water with backscatter set to 30 dB, a threshold of -120 dB was selected. A waveform was considered to originate from the ice surface if the peak power was less than -130 dB. Waveforms between these threshold values were rejected as complex.

Overall it is shown that, using a simple processing scheme, the instrument is capable of retrieving useful ice freeboard estimates even within single scenario runs. Optimum retrievals are obtained for ice concentrations between 90% and 95%

The percentage of water retrievals decreases and that of ice retrievals increases with increasing ice concentration. The corresponding error in the mean water elevation increases and that for the ice elevation decreases with increasing ice concentration. For water elevation, there is a clear relationship between ice concentration and retrieval accuracy. For ice elevation, it is apparent that lead orientation with respect to the ground track will plays a significant role, and hence the relationship to ice concentration is less definitive. However, these results would need much larger model runs with ground tracks with many different orientations to obtain a clearer statistical

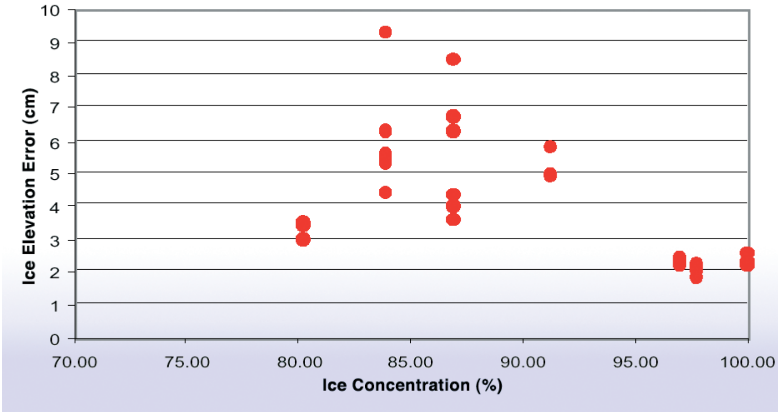

Figure 15. Simulated ice elevation errors versus ice concentration

picture. Varying the backscatter contrast has a marginal effect on water retrievals, but a significant effect on ice retrievals. This shows that a higher water/ice backscatter contrast can degrade ice retrievals in some instances, due to the interference of reflections from open water.

Overall, the simulations provide the first comprehensive and quantitative view of likely CryoSat performance under a variety of different ice conditions. The data sets generated will provide the basis for the development and optimisation of the sophisticated processing systems required for CryoSat level-1b and 2 processing.

4.3.2 Interferometric measurements for ice sheets

Figure 16 exhibits a scenario from a simulation experiment with SIRAL operating in SARIn mode over a typical glacier region in Antarctica. The instrument simulator provides typical waveforms and information on coherence and echo power. Results are shown on the left as typical one-dimensional plots for specific locations, showing echo power and inferred arrival angle as a function of range bin. In addition, the coherence is provided which quantifies the coherence of the wavefront arriving at the two antennas of the interferometer, and for these simulations it may be used as a proxy for the validity of the inferred arrival angle. The initial rise in coherence, coincident with the leading edge in the power trace, indicates that the corresponding inferred angle is unambiguous and valid. In these plots it is clear that the inferred arrival angle is providing useful information.

As an illustration, consider locations 0, 10 and 20, where the total surface slope (and, we assume, the across-track component as measured here) is, qualitatively speaking, respectively low, high and medium. The arrival angle of the leading edge in the corresponding echoes clearly shows the same relative behaviour.

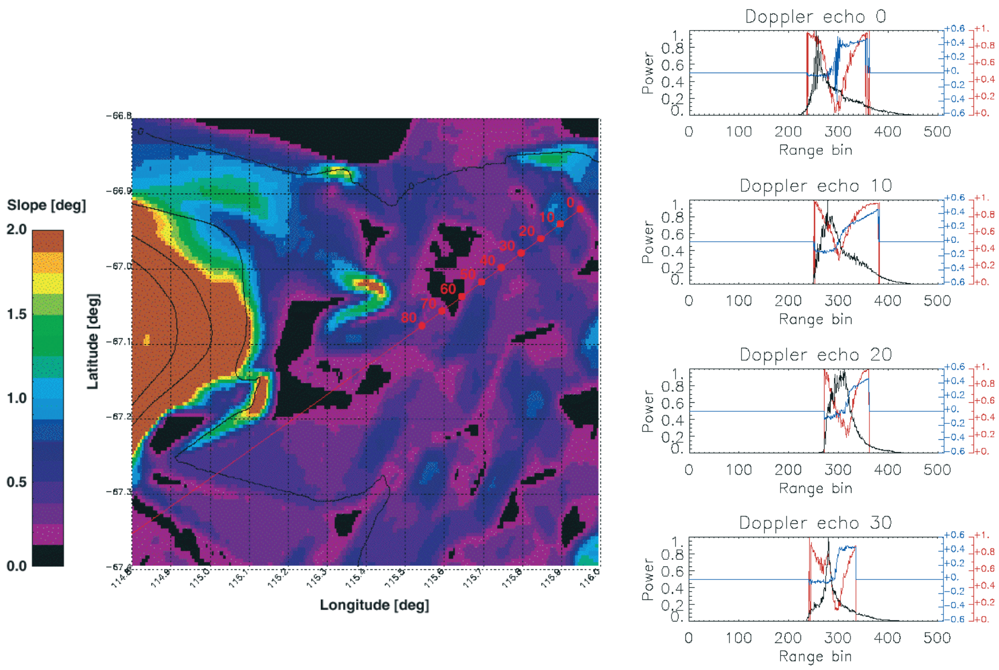

Figure 16. Simulations of the SAR-Interferometric mode of SIRAL with a DEM of Totten Glacier in Antarctica. The simulated echoes on the right are for locations 0-40 in the track plot. The black line indicates the echo power, the blue line the inferred arrival angle, and the red line the coherence. The magnitude of this value at the echo leading edge indicates where the inferred arrival angle is valid

4.4 Further error sources

In addition to the instrument simulations for typical topographic scenarios, further error terms need to be considered.

4.4.1 Sea surface topography uncertainty

Because the sea surface is smoothed on scales of 50 km, errors from the atmospheric corrections or the orbit are largely cancelled when determing a smoothed sea-surface topography along a certain instrument track (Fig. 6). However, unknown geoid and ocean topography on scales of less than 50 km introduces errors in the freeboard measurement. CryoSat will allow the derivation of a mean sea surface from its (largely) non-repeating tracks. The error at ~ 50 km from sea surface topography will be the difference between this mean surface and the actual sea surface at less than 50 km scales. A comparison with ground-based gravity of the Arctic mean sea-surface generated from the non-repeating ERS Geodetic Mission showed a slope error of 6×10^{-6} radians RMS, almost entirely at scales less than 35 km (Laxon & McAdoo

1998). The equivalent along-track mean sea-surface error is ~ 14 cm at 35 km. The mean dynamic topography in the Arctic is small, of order ~ 2 cm, so this error is largely that due to the measured mean sea surface. The variability of the dynamic topography Arctic Ocean is generally small, being of the order of 2 cm and dominated by large length scales. The error from this source will generally be small. In the Fram Strait, however, the short-scale topography associated with the East Greenland Current can be significant and an error of ~ 4 cm RMS may be introduced at monthly and 50 km scales (Peacock 1998). Tidal errors have large spatial scales and will be small.

4.4.2 Atmospheric refraction uncertainty

In general, the velocity of electromagnetic propagation is affected by the ionosphere, dry atmospheric mass, and atmospheric humidity (see e.g. Cudlip et al. 1994 and references therein). The largest effect is due to dry atmospheric mass for which the range error can be reduced to several millimetres by appropriate modelling. Any residual error is assumed to be small. The ionospheric correction is variable but small in polar regions. Also errors arising in long trends are considered to be insignificant. (Over Antarctica, the total correction is barely worth making.) The largest error is likely to be that that due to the atmospheric humidity, which can vary significantly in time and space. Most altimeter satellites carry a microwave radiometer to provide a measurement of water vapour. However, over ice surfaces this instrument does not provide accurate results. Thus CryoSat will not carry a radiometer and an atmospheric delay error will result. As Figure 17 shows, this error is likely to be of order 1.0 cm/year at 10^4 km^2 and 0.5 mm/year at 10^7 km^2.

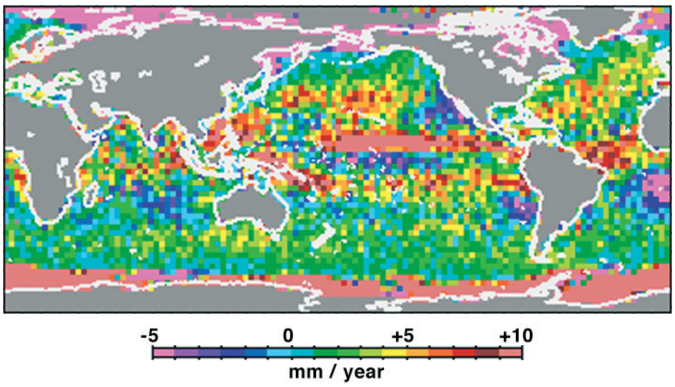

Figure 17. Wet troposphere errors. A comparison of modelled (ECMWF) and measured (MWR) wet tropospheric path delays for 3 years of ERS-2 data (1995-1998). The extremes of the colour bar are -0.5 and 1.0 cm/year. At high latitudes (except in regions of sea ice contamination of the MWR) the trends are very small, ~ 0.1 cm/year. A worst-case assumption is that trends at scales larger than 10^4 km^2 are independent, in which case the trends will be of order 0.3 cm/year at 10^4 km^2. At 10^7 km^2, we comfortably expect this error to be less than 0.05 cm/year. At latitudes higher than those shown, the correction becomes very small due to the low atmospheric temperatures

4.4.3 Orbit error

CryoSat's orbit will be determined from the measurements of the DORIS tracking system. These measurements are combined with models of gravitational forces and drag on the satellite to calculate the best estimate for its location. This procedure is complicated, but because of its general importance, a considerable literature exists on the subject of its errors (see, for example, Scharroo & Visser 1998). For the purposes of CryoSat, however, the most important feature of orbit errors is that they are dominated by fluctuations near the orbital period; they do not have a short-scale component. On the other hand, it is possible that longer-time-scale errors will arise, and these may have as much to do with uncertainties in the position of the Earth-fixed reference frame in which the DORIS measurements are made, as with the orbit itself. It is worth noting here that experience with the error of very high inclination and long repeat orbits such as for CryoSat is limited. Some forcing terms, such as the tidal forcing of the satellite, may need closer attention when account is taken of the effect of aliasing in the spatial averaging of the data. This matter deserves closer study. It is also worth noting that, even for a given satellite, the orbit error often improves with time as the force modelling of the satellite improves.

5 Data Products

CryoSat's principal output will be maps of variations in sea and land ice fluxes. The principal output of the SIRAL altimeter will be raw waveforms describing the surface reflection. A multi-stage processing chain is necessary to derive useful geophysical information from the raw data stream. Naturally, the processing chain splits for the different instrument modes.

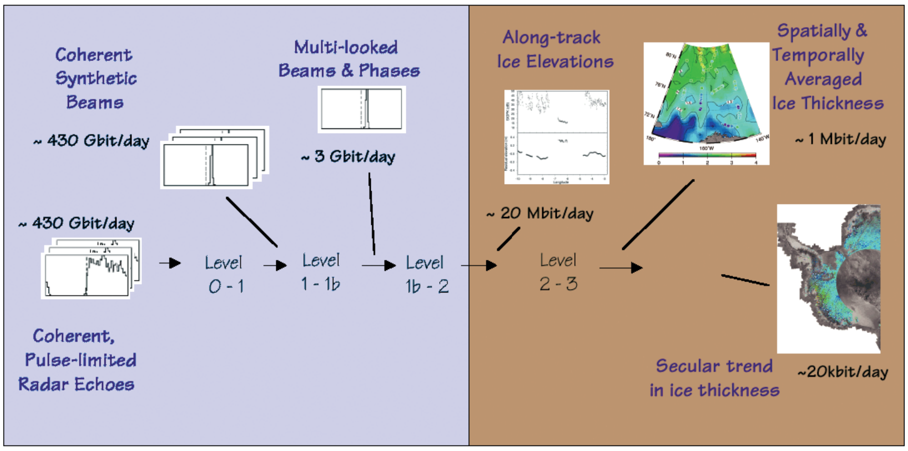

Figure 18. Principal processing chain for CryoSat

The following data products will be generated and stored in the Payload Data Segment (PDS):

- Level-0: raw telemetry source packets, filtered for errors, time ordered, and tagged with time and telemetry quality information; note that this includes instrument data, but also raw house-keeping telemetry parameters, to be forwarded to the FOS.
- Full-Bit-Rate (FBR): functionally the same information as Level-1b, but before the averaging on SAR and SARIn modes. The expected data volume will be very high, at 430 Gbit/day.
- Level-1b: containing instrument echo wave-forms; in the case of the SAR and SARIn operation modes, these wave-forms are averaged, so the data rate is much lower than the FBR above.
- Level-2: containing elevations along the orbit track.
- Scientific monitoring data: scientific performance of the SIRAL will be monitored systematically, resulting in e.g. trend plots, and statistical data

The provision of CryoSat data products requires numerous calibration and correction steps which are part of the processing chain, from a Level 0 up to a Level 2 data product. The different data levels are summarised in Table 5.

Data Type	Description	For the investigation of:	Data Volume
Full bit rate data (= Level 0 with housekeeping data removed)	Full engineering and geophysical corrected data with acquisition and other non-science data removed, and orbit and datation information added.	– Detailed scattering behaviour – Beam forming – Calibration – Instrument trouble-shooting	430 Gbit/day
Level 1b data	Full engineering and geophysical corrections applied. Beam formation and phase and amplitude multi-looking performed.	– Scattering behaviour – Elevation retrieval methods over land and sea ice – Calibration & Validation – Instrument trouble-shooting	3 Gbit/day
Level 2 data	Along-track elevation and backscattering 'coefficient' estimate.	– Ice fluxes and other geophysical phenomena – Validation	20 Mbit/day
Monitoring data	A subset of with degraded orbit and datation information.	– Instrument health – Instrument long-term monitoring	5 Mbit/day

Table 5. CryoSat data products

5.1 Level 0: Full bit rate data

The aim of the ESA ground segment is to generate elevation estimates from the CryoSat data. To do so, considerable compression of the information content of the data is required without losing the inherent geophysical information during these processing steps. Because the SIRAL is an experimental sensor, it is likely that the algorithms used in the compression will need to be modified in the light of experience gained after launch and during Cal/Val campaigns. Such a reconfiguration will require lower level data. The FBR data are the highest level data in which the full information content of the acquired data is retained.

5.2 Level 1b: Single combined waveform data

Level 1b data consists, essentially, of an echo for each point along the ground track of the satellite. As with the full bit rate data, the Level 1b data are needed to investigate in detail the algorithms that are used to generate the elevation estimates of the Level 2 data. In contrast to the FBR data, the Level 1b data are compressed with respect to the acquired data, which allows them to be used over fairly large time and space scales. They are also the highest level data that may be obtained without geophysical approximations. However, geophysical corrections on processes that have an influence on the data quality have been applied, including:

- Corrections for ionosphere, dry and wet atmosphere
- Ocean and solid-Earth tide effects
- EM bias correction
- Inverse barometer correction.

Depending on the instrument mode, the data records for Level 1b and Full-bit-rate will differ, providing all specific mode parameters needed for processing to higher data levels. This includes information on coherence and phase angle for the SARIn mode, as well as a general beam behaviour description for the synthetic aperture processing. The precise content of this beam parameter is still to be defined. These additional parameters will be available after the Level 1b processing stage. For all modes, the echo waveform will be provided with a resolution of 128 range gates.

5.3 Level 2: Along-track elevation

Level 2 data consist, essentially, of estimates of the elevation of successive points along the ground-track of the satellite. The along-track sampling rate will be 1 sec. Along-track elevations are the lowest level data that may be applied directly to a geophysical problem. At least in principle, they are also the lowest level data for which detailed understanding of the radar signal processing is not required. Level 2 data will be the basis for any further scientific exploitation outside the ESA Ground Segment and the production of higher data levels like temporal or spatial trend estimations. Depending on the instrument mode, this data will have varying spatial resolutions. In pulse-limited operation, the circular footprint will be similar to that of any other conventional altimeter and in the order of several kilometres. For the SAR- and SARIn modes, the along-track resolution will be 250 m whereas across-track it will be equal to the antenna footprint of up to 15 km. The backscatter signal amplitude will be provided as a σ_0 value. For the SARIn mode, the across-track angle of the first echo return will be available.

5.4 Monitoring data

Monitoring data will provide timely information on the health of the payload. It consists of a set of parameters whose values should be determined rapidly and routinely, i.e. for every orbit. It will also provide engineering information, additional to that in the science data stream in the event of unexpected anomalies.

5.5 Data distribution

There is no need for near real time delivery of CryoSat data, except for specific needs during calibration or validation activities. For Level 1 and 2 data, it will be possible for the user to order data by describing a space-time window. Tailored software for data access and conversion will be provided. Data distribution will be on CD-ROM discs and via FTP transfers where feasible.

Table 6 summarises the distribution requirements. Data latency is the time delay between data acquisition and distribution. The min/max durations specify the minimum and maximum intervals of continuous satellite operation for which a data product is available.

Data	Latency	Minimum Duration	Maximum Duration	Users
Full bit rate data	< 1 week	10 min	10 min	Cal/Val teams, subject to resource limitations
Level 1b	< 1 week	10 min	none	Cal/Val teams & requests from data exploitation AO
Level 2	< 1 week	1 orbit	none	Cal/Val teams & requests from data exploitation AO

Table 6. CryoSat data distribution requirements

6 The Ground Processing Concept

6.1 General architecture

To process and store the data products the Ground Segment is implemented in several segments which have dedicated functionalities (Fig. 19):

- The Flight Operations Segment (FOS) is responsible for the mission planning, command and control, and telemetry acquisition. The mission planning includes spacecraft maintenance activities and planning of the radar altimeter mode changes. The satellite command and control is responsible for all flight operations and the instrument management. Instrument commands are merged with the spacecraft maintenance commands and up-linked to the satellite by the Kiruna Ground Station; recorded telemetry is also acquired at Kiruna, to monitor satellite health, and provide scientific data to the processing chain.
- The Payload Data Segment (PDS) is responsible of all scientific data processing, archiving and distribution. All data products required are generated and archived at Kiruna during the mission. Routinely, only the Level-2 data products, amounting to a few Mbytes per day, are distributed to the scientific community. The facility implemented at Kiruna will be configured such that access to the data for eventual duplication of the archive at national centres is possible. Furthermore, the infrastructure shall allow for at least one overall reprocessing of the data if needed during the exploitation phase.
- Complementary elements, potentially shared with other missions, include the User Services Facility as the interface and help desk for the scientific users and the Long-Term Archive.

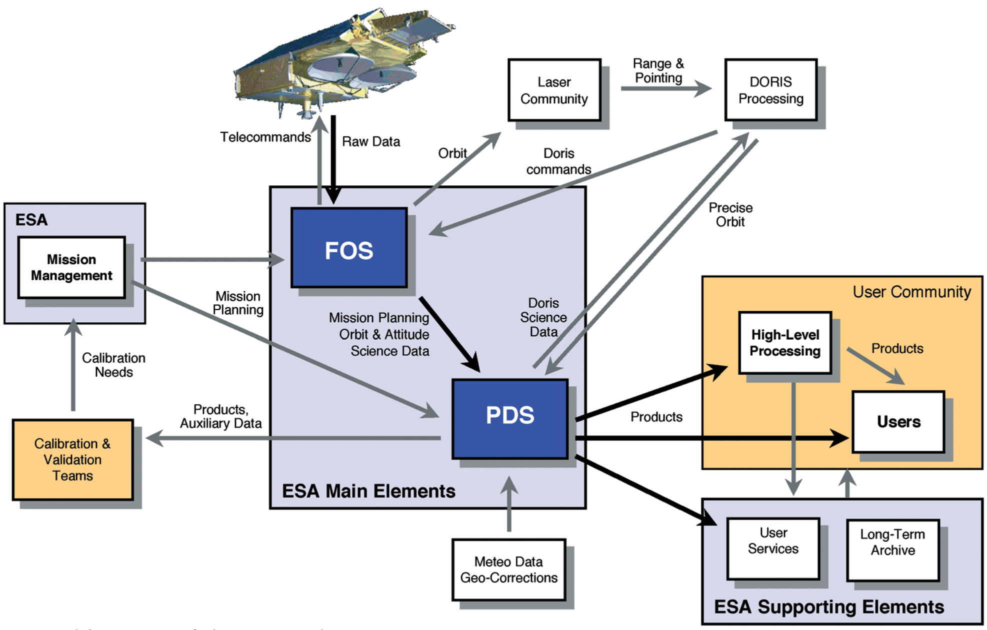

Figure 19. Architecture of the Ground Segment

6.2 Mission management

The mission planning consists mainly of two elements: flight operation of the satellite including possible orbit changes (validation and science orbits), and instrument mode switching for different observation areas. The pulse-limited SAR and SARIn operation modes will be controlled by a geographical mask and possible manual control. The mask can be adapted weekly to take into account seasonal variations of sea ice cover in both hemispheres. Figure 20 shows a worst-case scenario with maximum sea ice extend in the Arctic and Antarctic. Even with this unrealistic assumption, the on-board storage and download capabilities are large enough to deal with this scenario. Manual control and temporary overriding of this mask is possible for special validation campaigns or certain experimental requests in later phases of the mission’s lifetime.

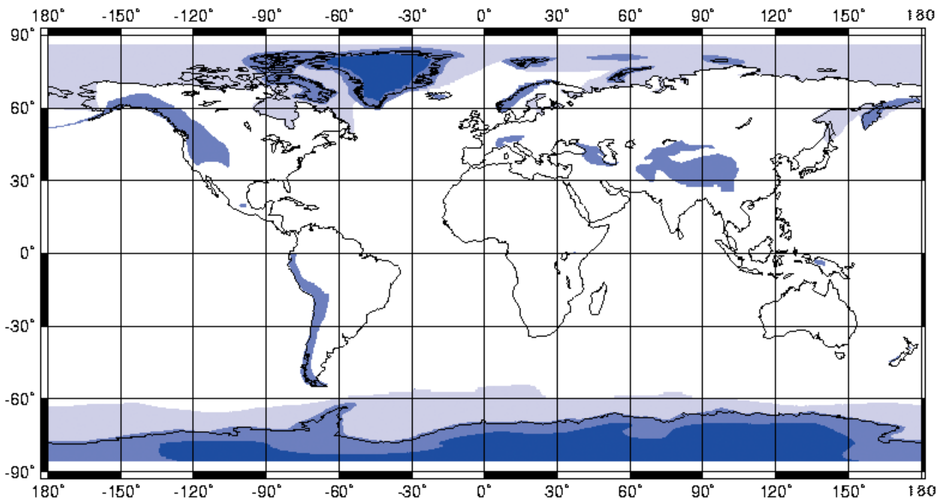

Figure 20. Geographical mask which determines the SIRAL operation modes. Dark blue and white: low resolution pulse-limited mode. Medium blue: SARIn mode for ice sheets and glaciers. Light blue: sea ice regions

7 SIRAL Data Validation

7.1 General requirements

In Chapter 4 a simple approach has been used to derive a first guess for the vertical accuracy from the single shot measurements, assuming an average mass rate change $\overline{\sigma}$ per unit area. To derive more precise requirements for calibration and validation activities, it is necessary to revisit in more detail the fundamental objective of CryoSat to observe mass rate changes for land ice or floating sea ice areas and to consider the thickness changes $\dot{h}$ rather than a mass rate. In general, the mass rate will be a function of space $\boldsymbol{x}$ and time t. Here $\boldsymbol{x}$ should be understood as a vector co-ordinate describing a location on the Earth's reference figure. Generally, the mission aims to make estimates of $\dot{h}$ averaged over an area A. Over land ice, A may typically be a drainage basin; over sea ice A may be a 10^5 km^2 region whose trends may usefully be compared with the numerical model. The trends will also be averaged over a time interval T that will typically be the mission duration, but may be shorter if the annual cycle is of interest, or longer if historical altimeter data can also be brought to bear. The general objective is therefore to measure an average trend. In practice the function $h(\boldsymbol{x},t)$ is not continuous, but is determined by discrete measurement locations $\boldsymbol{x}_i$. In practice, a continuous description of the average trend is approximated by local spatial averages, and there are two approaches for doing this:

$$\overline{\dot{h}} \sim \frac{1}{AT} \int_A dA \sum_i w_i(\boldsymbol{x}) \left(h(\boldsymbol{x}_i, t_1 + T) - h(\boldsymbol{x}_i, t_1) \right)$$

or (4)

$$\overline{\dot{h}} \sim \frac{1}{T} \left(\frac{1}{A} \int_A dA \sum_i w_i(\boldsymbol{x}) h(\boldsymbol{x}_i, t_1 + T) - \frac{1}{A} \int_A dA \sum_j w_j(\boldsymbol{x}) h(\boldsymbol{x}_j, t_1) \right)$$

where the w are the quadrature (numerical integration) weights. The distinction between the two possibilities is that in the first case the quadrature errors are cancelled by insisting that the observations lie at the same discrete locations. In the second, the estimated trend contains the difference in quadrature errors, but the measurements are not restricted to lie at the same location. In the case of land ice, the change in thickness is small in comparison with the elevation. Experience shows that the observations need to be at the same locations. (This is achieved in practice using the method of orbit cross-overs). On the other hand, such an approach is not available in the case of sea ice because the locations of the sea ice freeboard measurements are not known *a-priori* (they depend on the locations of the ice floes), and the second form of Equation (4), is used.

With this proviso, it is assumed that the sampling density of the land and sea ice will be sufficient to suppose that (for a sensible choice of *w*) the quadrature errors will be negligible, so that we can take

$$h(\boldsymbol{x},t_1 + T) - h(\boldsymbol{x},t_1) = \sum_i w_i(\boldsymbol{x})(h(\boldsymbol{x}_i,t_1 + T) - h(\boldsymbol{x}_i,t_1))$$

and (5)

$$h(\boldsymbol{x},t) = \sum_i w_i(\boldsymbol{x})h(\boldsymbol{x}_i,t_i)$$

in the cases of land ice and sea ice, respectively.

In general, measurements for a location $\boldsymbol{x}_i$ will be in error by an amount σ which may be a local average of single shot measurement errors $\sigma_{i'}$. The local approximations to the land ice elevation change or sea ice thickness will then contain errors that are, respectively,

$$\Delta(x,t_1,T) = \sum_i w_i(x)(\sigma(x_i,t_i + T) - \sigma(x_i,t_1)) \tag{6}$$

and

$$\varepsilon(x,T) = \sum_i w_i(x)(\sigma(x_i,t_i)) \tag{7}$$

since by assumption the quadrature errors are negligible. To put it another way, one can assume that the error of significance is that associated with the measurements, rather than that associated with a lack of them. In line with the above remarks, these expressions for the errors Δ or ε may be taken as a shorthand for errors that refer, for example, to an average of observations over some short time interval, or to a curve-fitted trend rather than a difference of end points.

The second moments of the spatially averaged measurement errors are the quantities

$$E\{\bar{\dot{\varepsilon}}^2\} = \left(\tfrac{1}{AT}\right)^2 \int_A dA \int_A dA' E\{\Delta(\boldsymbol{x},t_1,T)\Delta(\boldsymbol{x}',t_1,T)\}$$

or (8)

$$E\{\bar{\dot{\varepsilon}}^2\} = \left(\tfrac{1}{AT}\right)^2 \int_A dA \int_A dA' E\{(\varepsilon(\boldsymbol{x},t_1+T) - \varepsilon(\mathrm{x},t_1))(\varepsilon(\boldsymbol{x}',t_1+T) - \varepsilon(\boldsymbol{x}',t_1))\}$$

in the cases of land ice and sea ice, respectively. Here $E\{\cdot\}$ denotes expectation.

The task of calibration and validation is to estimate by independent measurement the expectations of Equation (8). Since these are generally a function of $\boldsymbol{x}$, $\boldsymbol{x}'$, t_1 and T, with all that this implies for the space-time sampling of experiments, one of the main purposes of a Cal/Val strategy is to reduce the complexity of the problem by simplifying the expectation, mainly by appealing to empirical knowledge.

The preceding discussion is of a rather general nature. Nonetheless, a number of important features of the calibration and validation problem for CryoSat can be deduced from it.

The first feature is that, because an objective of the mission is to measure a trend, validation experiments will need to be repeated. For a mission lifetime of 3-5 years' duration, it will scarcely be possible to gain sufficient samples to estimate the temporal covariance function. Indeed, given that the errors are seasonally variable, only a few temporal measurements are possible. However, the difference in the character of the land- and sea-ice covariance functions places a different emphasis on the nature of the repetition.

The second feature is that, because an objective of the mission is to measure a spatial average, it is the spatial *co*variance, and not simply the variance of the error that needs to be estimated. While it *may* be possible in the case of sea ice to estimate the covariance of the thickness error from a single temporal sample, this is still a function of space, and estimating it requires many measurements. The covariance function has a structure that may be hidden in a point spatial measurement. In consequence, a point measurement may offer little information as to the error in the spatial average. In practical terms, the source of most of the short scale error is the speckle on the radar echoes. Independent measurements that are dominated by radar speckle are of limited use unless there are a sufficient number to average out the speckle fluctuations. This makes the land ice problem particularly challenging in practice, because it is the correlation function of the temporal difference in elevation *at the same locations* that is required. It is not sufficient to make measurements in the same region at different times; they must be at numerous, *identical* locations at different times.

A detailed discussion on the consideration of all possible error terms and appropriate validation methods can be found in the CryoSat Calibration and Validation Concept (ESA 2001)

7.2 Pre-launch activities

In preparation for all calibration and validation activities, an official Announcement of Opportunity was released in November 2001. Scientists were invited to propose campaigns and experiments relevant to the Cal/Val objectives of the mission. More than 20 proposal had been received by the closing date in April 2002. The established calibration, validation and retrieval team consists of scientists from many European countries and the USA. Numerous kinds of measurements will be prepared and conducted from ships, airplanes and stationary ice camps.

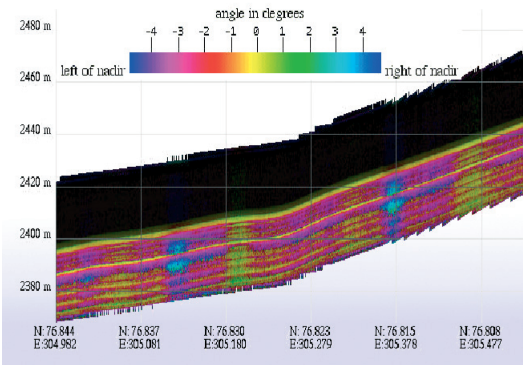

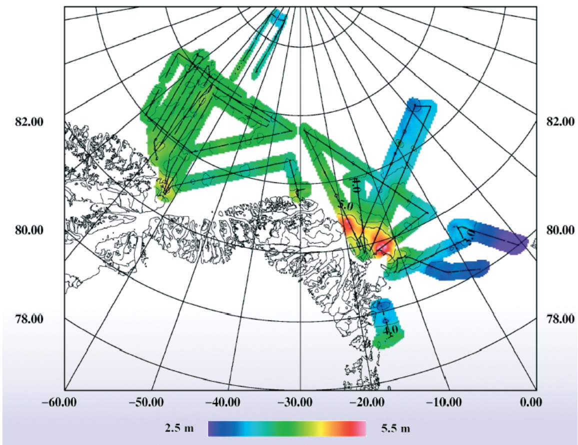

Figure 21. Results from first CryoSat validation campaigns. Left: Radar profile from LaRa with SARIn processing indicating reflections from different snow/ice layers (Raney et al. 2002). Right: Sea ice thickness estimations along flight tracks of ESAG (Forsberg et al. 2002)

In 2002, two campaigns served as precursor activities providing the first valuable in-situ data sets for the CryoSat data validation. In cooperation with US scientists and their flight programme for validation of NASAs ICEsat satellite, several tracks could be measured over central Greenland and surrounding sea ice areas (Experiment Lara, Raney et al. 2002). The instrumentation consisted of a scanning laser altimeter and the Ku-band JHU-APL radar altimeter, which allows interferometric SAR processing similar to the CryoSat concept. For the first time, collocated laser and radar-profiles for ice surfaces could be obtained, which is a beneficial asset for the validation studies (Fig. 21, left). Another flight campaign (ESAG, Forsberg et al. 2002) has been conducted by a Danish science team, obtaining a comprehensive set of laser topographic profiles for sea ice regions in the Fram Strait and north of Greenland

(Fig. 21, right). These kinds of activities will continue in the coming years in accordance with the overall validation strategy.

7.3 In-flight calibration

The satellite system is provided with a number of ancillary measurement modes and equipment whose purpose is to provide an independent measurement of the system errors. In some cases, these also provide on-going measurements that are then used to make corrections to the raw data. These measurements separate into two approaches, depending on which part of the instrument system is being investigated. The radar contains a calibration path which injects the transmitted signal directly into the receiver chain immediately downstream of the antenna. All instrument time and phase paths within this internal loop may be measured in this way – so-called ‘internal’ calibration modes. However the antennas of the radar system cannot be measured this way. In addition, it is not possible from internal measurements to establish the error in position and attitude with respect to an Earth-fixed reference frame. Both of these system elements require an externally generated signal incident on the antenna – so-called ‘external calibration’.

Error	Pre-launch Testing	Internal Calibration	External Calibration
Echo Timing	Yes	Yes	No
Echo Datation	No	No	Yes
Satellite Altitude	No	No	Yes
Total Echo Power	Yes	In part	Yes
Echo Shape	Yes	Yes	No
Baseline Vector	In part	No	Yes
Interferometer Phase	In part	In part	No

Table 7. Internal and external calibration of Level 1b data

A summary of the breakdown of internal and external calibration requirements is given in Table 7. Also included are those elements that will be the subject of pre-launch measurements and characterisation. In general, pre-launch measurements will determine absolute offsets (e.g. that between the nominal and actual star tracker axes). Internal calibration measurements are instructed under ground command. These can therefore sample a wide range of time scales. Typically, a high temporal density of internal calibrations is used early in the mission to establish the behaviour on, for example, orbital time scales, and a lower number is used thereafter.

A summary of the planned approach to external calibration is given in Table 8. These may be divided, from a temporal sampling point-of-view, into two cases. External calibration of the echo direction will be performed using a specific measurement mode over the ocean surface. So long as the satellite is over the ocean, this measurement mode can be controlled by ground command. Like internal calibration, it too can span a wide range of time scales.

Error	Technical Approach	Mission Variability Requirement	Mission Bias Requirement
Echo datation	Transponder	2 m	None
Satellite Altitude	Laser Retroreflector	3 cm	0.17 cm/yr
Total Echo Power	Transponder	3 dB	0.05 dB/yr
Baseline Vector	Ocean Surface	10″	None
Interferometer Phase	Transponder	6″	None

Table 8. External calibration approach and estimated magnitudes

Note that it will not be possible to separately calibrate the baseline attitude and the interferometer phase error, but only the combined effect of these on the echo direction measurement. The ‘calibration’ of the satellite altitude is performed through laser retro-reflector measurements. These depend to some extent on the availability of the laser measurements. At the time of writing, this is not well established. The term ‘calibration’ is put in inverted commas here because there is an inevitable tendency to use the laser measurements within the orbit computation once they become available. Nonetheless, they do provide an accurate and independent check on the point variability of the orbit deduced from the RF DORIS measurement system.

Finally, there are measurements that require transponders. These cannot provide such dense temporal sampling, because the satellite must overfly the transponder locations. It is expected that such measurements will be performed in the validation phase.

Transponder measurements also offer a very effective way of checking out the lower level processing of the data such as, for example, the directional accuracy of individual beams prior to multi-looking.

References

Aagaard, K., 1994, “The Arctic Ocean and Climate: A Perspective”, Geophysical Monograph **85**, 5 - 20, American Geophysical Union.

Aagaard, K. & E.C. Carmack, “The role of sea ice and other fresh water in the Arctic circulation”, J. Geophys. Res., **94**, 14485 - 14498.

ACSYS, 1998, “ACSYS Implementation and Achievements”, acsys.npolar.no/impplan/index.html.

Alley, R.B. & I.M. Whillans, 1991, “Changes in the West Antarctic Ice Sheet”, Science, **254**, 959 - 963.

Arthern, R.J., 1996, Ph.D. Thesis, University of London.

Beltley, C.R. & M.B. Giovinetto, 1991, “Mass balance of Antarctica and sea-level Change”, in Role of the Polar Regions in Global Change, University of Alaska, Fairbanks, pp 481 - 488.

Bertiger, Y.E. & 19 co-authors, 1994, “GPS precise tracking of TOPEX/Poseidon: Results and implications”, J. Geophys. Res., **99**, 24449 - 24464.

Bleck, R., C. Rooth, D. Hu, & L.T. Smith, 1992, Salinity-driven thermocline transients in a wind- and thermohaline-forced isopycnic coordinate model of the North Atlantic. J. Phys. Oceanogr. **22**, 1486 - 1505.

Bjørgo, E., O.M. Johannessen & M.W. Miles, 1997. Analysis of merged SMMR/SSMI time series of Arctic and Antarctic sea ice parameters. Geophys. Res. Lett. **24**, 413 - 416.

Bilitza, D., C. Koblinsky, B. Beckley, S. Zia & R. Williamson, 1995, “Using IRI for the computation of ionospheric corrections for altimeter data analysis”, Advances in Space Research, **15**, 113 - 119.

Bond, G., W. Broecker, S. Johnsen, J. McManus, L. Labeyrie, J. Jouzel & G. Bonani, 1993, “Correlations between climate records from North Atlantic sediments and Greenland ice”, Nature, **365**, 143 - 147.

Broecker, W.S., 1994, “Massive iceberg discharge as triggers for global climate change”, Nature, **372**, 421 - 424.

Cavalieri, D.J., P. Gloersen, C.L. Parkinson, H.J. Zwally & J.C. Comiso, 1997, Observed hemispheric asymmetry in global sea ice changes, Science, **278**, 1104.

Chao, B.F., 1994, “Man-made lakes and sea-level rise”, Nature, **370**, 258.

Colman, R.A., S.B. Power, B.J. MacAveney & R.R. Dahni, 1995, “A non-flux corrected transient CO_2 experiment using the BMRC coupled ocean atmosphere GCM”, Geophys. Res. Lett., **22**, 3047 - 3050.

Comiso, J.C., P. Wadhams, W.B. Krabill, R.N. Swift, J.P. Crawford & W.B. Tucker, 1991, “Top/Bottom Remote Sensing of Arctic Sea Ice:, J. Geophys. Res., **96**, 2693 - 2709.

Cubash, U., K. Hasselmann, H. Hock, E. Maier-Reimer, U. Mikolajewicz, B.D. Santer & R. Sausen, 1992, “Time dependent greenhouse warming computations with a coupled ocean-atmosphere model”, Clim. Dyn., **10**, 1 - 19.

Cudlip, W. & 12 co-authors, 1994, “Corrections for altimeter low-level processing at the earth Observation Data Centre”, Int. J. Remote Sensing, **15**, 889 - 914.

Dickson, R.R., J. Meincke, S.-A. Malmberg & A.J. Lee, 1988, The “Great Salinity Anomoly” in the Northern Atlantic 1968 - 1982”, Prog. Oceanography, **20**, 103 - 151.

Eicken, H., M. Lensu, M. Lepparanta, W.B.Tucker III, A.J. Gow & O. Salmela, 1995 “Thickness, structure and properties of level summer multi-year ice in the Eurasian sector of the Arctic Ocean”, J. Geophys. Res., **100**, 22697 - 22710.

Enomoto, H., 1991, “Fluctuations of snow accumulation in the Antarctic and sea-level pressure in the Southern Hemisphere in the last 100 years”, Climatic Change, **18**, 67 - 87.

ESA, 1996, “The Topography Mission: Report for Assessment”, ESA SP-1196(9).

ESA, 1998, The Earth Explorer Programme: The Science and Research Element of ESA’s Future Earth Observation Program”, ESA-SP-1227.

ESA, 2001: Cryosat Calibration and Validation Concept, CS-PL-UCL-SY-0004, European Space Agency, 91 pp.

Farrell, W.E. & J.A. Clarke, 1976, “On post-glacial sea-level”, Geophys. J. Roy. Astron. Soc., **46**, 647 - 667.

Fischer, H. & P. Lemke, 1991, “On the required accuracy of atmospheric forcing fields for driving dynamic-thermodynamic sea ice models”, in Geophysical Monograph, **85**, 373 - 381, American Geophysical Union.

Fetterer, F.M., M.R. Drinkwater, K. Jezek, S. Laxon, R.G. Onstott & L. Ulander, 1992, "Sea Ice Altimetry" in Microwave Remote Sensing of Sea Ice, (F. Carsey ed.), AGU Geophys. Monograph, **68**, 111 - 135.

Flato, G.M. & W.D. Hibler, 1992, "Modeling pack ice as a cavitating fluid", J. Phys. Ocean., **22**, 626 - 651.

Forsberg, R., S. Ekholm, K. Keller & D. Burtin, 1992, "GPS measurements in Greenland in support of gravity measurements and satellite altimetry", Proc. 6th Int. Symp. on Satellite Positioning, Columbus, Ohio, 905 - 914.

Forsberg, R., K. Keller, S.M. Hvidegaard & A. Olesen, 2002: European Airborne Gravity and Lidar Survey in the Arctic Ocean, Final ESA Report, 28 pp.

Gates, W.L. & 9 co-authors, 1996, "Climate Models - Evaluation", in Climate Change 1995, The Science of Climate Change, Cambridge University Press.

Gloersen, P., W.J. Campbell, D.J. Cavalieri, J.C. Comiso, C.L. Parkinson & H.J. Zwally, 1992, Arctic and Antarctic Sea Ice, 1978-1987: Satellite Passive-Microwave Observations and Analysis, NASA SP-511, NASA, Washington DC, 1992.

Gogineni, S., R.K. Moore, Q. Wang, G.A. & R.G. Onstott, 1990, Radar backscatter measurements over saline ice, Int. J. R. Sensing **11** (4), 603 - 615.

Gordon, A.L. & J. Comiso, 1988, Polynyas in the Southern Ocean, Scientific American, 256, 6, 90 - 97.

Gornitz, V., S. Lebedeff & J. Hansen, 1982, "Global Sea Level Trends in the Past Century", Science, **215**, 1611 - 1614.

Gorshkov, S.G., 1983, World Ocean Atlas, Vol. 3, Arctic Ocean, Pergammon, New York.

Grey, J.M.N. & L.W. Morland, 1994, "A two-dimensional model for the dynamics of sea ice", Phil. Trans. Proc. Roy. Soc. Lond., **347**, 219 - 290.

Haeberli, W. & M. Hoelzle, 1995, "Application of inventory data for estimating characteristics of and regional climate change effects on mountain glaciers - a pilot study with the European Alps", Ann. Glaciology, **21**, 206 - 212.

Hakkinen, S. & G.L. Mellor, 1992, "Modeling the seasonal variability of a coupled Arctic ice-ocean system", J. Geophys. Res., **97** (C12), 20285 - 20304.

Hansen-Bauer, I., 1992, “The Climate of Halley - Antarctica”, DNMI Report, No. 3/92 Aurora and 26/92 Klima, 22 pp.

Harder, M., P. Lemke & M. Hilmer, 1998, “Simulation of sea ice transport through Fram Strait : Natural variability and sensitivity to forcing”, J. Geophys. Res., **103**, 5595 - 5606

Hibler, W.D., 1979, “A dynamic thermodynamic sea ice model”, J. Oceanography, **9**, 815 - 846.

Hibler, W.D., 1986, “Ice dynamics” in The Geophysics of Sea Ice, NATO ASI Ser., Ser. B Phys., vol. **146**, (ed. N. Untersteiner), 577 - 640, Plenum, New York.

Hibler, W.D. & K. Bryan, 1987, “A diagnostic ice-ocean model”, J. Phys. Oceanogr. **17**, 987 - 1915.

Horel, J.D. & J.M. Wallace, 1981, “Planetary scale atmospheric phenomena associated with the interannual variability of sea surface temperatures in the equatorial Pacific”, Mon. Weather Rev., **109**, 813 - 829.

Hughes, T., 1981, “The weak underbelly of the West Antarctic Ice Sheet”, J. Glaciology, **27**, 518 - 525.

Hunke, E.C. & J.K. Dukowicz, 1997, “An elastic-viscous-plastic model for sea ice dynamics” J. Phys. Oceanogr. **27** (9), 1849 - 1867.

Huybrechts, P., 1990, “A 3-D model for the Antarctic Ice Sheet: a sensitivity study on the glacial-integlacial contrast”, Climate Dynamics, **5**, 79 - 92.

Huybrechts, P., 1994, “The present evolution of the Greenland Ice Sheet: an assessment by Modeling”, Global Planetary Change, **9**, 39 - 51.

Ip, C.F., W.D. Hibler & G.M. Flato, 1991, “On the effect of rheology on seasonal sea ice simulations”, Ann. Glaciology, **15**, 17 - 25.

IPCC, 2001, Intergov. Panel on Climate Change: Climate Change 2001, The Scientific Basis, http://www.grida.no/climate/ipcc_tar/wg1/index.htm

Jacobs, S.S, H.H. Helmer, C.S.M. Doake, A. Jenkins & R.M. Frolich, 1992, “Melting of ice shelves and the mass balance of Antarctica”, J. Glaciology, **38**, 375 - 387.

Jensen, J.R. & R.K. Raney, 1998, Delay/Doppler Radar Altimeter: Better Measurement Precision, Proceedings IEEE International Geoscience and Remote Sensing

Symposium IGARSS'98, Seattle, Washington, USA, IEEE No. 98CH36174, July 1998, 2011 - 2013.

Jensen, J.R. & R.K. Raney, 1996, Multi-Mission Radar Altimeter: Concept and Performance, Proceedings IEEE International Geoscience and Remote Sensing Symposium IGARSS'96, Lincoln, Nebraska, USA, IEEE No. 98CH36174, May 1996, 2011 - 2013.

Johannessen, O.M., M. Miles & E. Bjorno, 1995, "The Arctic's shrinking sea ice", Nature, **367**, 126 - 127.

Kreyscher, M., M. Harder, P. Lemke & G.M. Flato, 2000, "Results of the sea ice model intercomparison project: Evaluation of sea ice rheology schemes for use in climate simulations", J. Geophys. Res., **105** (C5), 11299 - 11320.

Kwok, R., J.C. Curlander, R. McConnell & S.Pang, 1990, An ice-motion tracking system at the Alaska SAR Facility, IEEE J. of Oceanic Engineering, Vol **15**, No 1.

Laxon, S.W. & D. McAdoo, 1994, "Arctic Ocean gravity field derived from ERS-1 satellite altimetry", Science, **256**, 621 - 624.

Laxon, S.W. & D. McAdoo, 1998, "Satellites provide new insights into polar geophysics", EOS Trans., **79**, 69 - 73.

Laxon, S.W., S. Sandven & H. Drange, 2001, "The quantification of the importance of the sea ice budget in the climate system", ESA Study Report 13971/00/NL/DC.

Legresy, B. & F. Remy, 1998, "Using the temporal variability of satellite radar altimetric observations to map surface properties of the Antarctic Ice Sheet", J. Glaciology, **44**, 147**,** 197 - 206.

Lemke, P., W.B. Owens & W.D. Hibler III, 1990, "A coupled sea ice mixed layer pycnocloine model for the Weddell Sea", J. Geophys. Res. **95**, 9513 - 9525.

Le Meur, D.E. & P. Huybrechts, 1998, "Present-day uplift patterns over Greenland from a coupled ice sheet / visco-elastic bedrock model", Geophys. Res. Lett., **25**, 3951 - 3954.

MacAyeal, D.R., 1992, "Irregular oscillations of the West Antarctic Ice Sheet", Nature, **359**, 29 - 32.

Manabe, S. & R.J. Stouffer, 1988, "Two stable equilibria of a coupled ocean-atmosphere model", J. Climate, **1**, 841 - 866.

Manabe, S., R.J. Stouffer, M.J. Spelman & K. Bryan, 1991, "Transient Responses of a Coupled Ocean-Atmosphere Model to Gradual Changes of Atmospheric CO_2. Part 1: Annual Mean Response", J. Climate, **4** , 785 - 818.

Marth, P.C., J.R. Jensen, C.C. Kilgus, J.A. Perschy, J. L. MacArthur, D.W. Hancock, G.S. Hayne, C.L. Purdy, L.C. Rossi, & C.J. Koblinsky, 1993, Prelaunch Performance of the NASA Altimeter for the TOPEX/Poseidon Project, IEEE Transactions on Geoscience and Remote Sensing, **31**, No. 2, 315 - 332.

Martin, T.V., H.J. Zwally, A.C. Brenner & R.A. Bindschadler, 1983, "Analysis and retracking of continental ice sheet radar altimeter waveforms", J. Geophys. Res., **88**, 1608 - 1616.

Maykut, G.A. & N. Untersteiner, 1971, "Some results from a time-dependent thermodynamic model of sea ice", J. Geophys. Res., **76**, 1550 - 1575.

McAdoo, D. & S.W. Laxon, 1997, "Antarctic tectonics: Constraints from an ERS-1 Satellite Marine Gravity Field", Science, **276**, 556 - 560.

McLaren, A.S., J.E. Walsh, R.H. Bourke, R.L. Weaver & W. Wittmann, 1992, "Variability in sea ice thickness over the North Pole from 1977-1990", Nature, **354**, 224-226.

McLaren, A.S., R.H. Bourke, J.E. Walsh & R.L. Weaver, 1994, "Variability in sea ice thickness over the North Pole from 1958-1992", Geophysical Monograph **85**, 363 - 371, American Geophysical Union.

Meier, M.F., 1984, "Contribution of small glaciers to global sea-level", Nature, 343, 115 - 116.

Meier, M.F. & D.B. Bahr, 1996: Counting glaciers: use of scaling methods to estimate the number and size distribution of the glaciers of the world. pp. 89-94 in Glaciers, Ice Sheets, and Volcanoes: A Tribute to Mark F. Meier, ed. S. C. Colbeck. U.S. Army Corps of Engineers, Cold Regions Research and Engineering Laboratory (CRREL),New Hampshire, USA.

Melbourne, W.G., E.S. Davis, T.P. Yunck & B.D. Tapley, 1994, "The GPS flight experiment on TOPEX/Poseidon", Geophys. Res. Lett., **21**, 2171 - 2174.

Monterfredini, E., F. Morelli, G. Picardi & R. Seu, 1995, "A non-coherent surface backscattering model for radar observation of planetary bodies and its application to Cassini radar altimeter", Planetary and Space Science, **43**, Elsevier Science Ltd.

Murphy, J.M. & J.F.B. Mitchell, 1995, “Transient Response of the Hadley Centre Coupled Model to increasing carbon dioxcide. Part II. Temporal and Spatial evolution of patterns”, J. Climate, **8**, 57 - 80.

Nakada, M. & K. Lambeck, 1988, “The melting history of the late Pleistocene Antarctic ice sheet”, Nature, **333**, 36 - 40.

Oberhuber, J.M., 1992, “The OPYC Ocean General Circulation Model”, Tech. Rep. 7, D. Klimarechenzentrum GmbH, Hamburg, Germany.

Parashar, S.K., A.W. Biggs, A.K. Fung & R.K. Moore, 1974, “Investigation of radar discrimination of sea ice” In Proc. 9th International Symp. on R. Sensing of the Environment, Ann Arbor, MI, 323-332.

Parkinson, C.L. & W.M. Washington, 1979, “A large-scale numerical model of sea ice”, J. Geophys. Res. **84**(C1), 311 - 337.

Peacock, N.R., 1998, Ph. D. Thesis, University of London.

Peacock, N.R., S.W. Laxon, R. Scharoo & W. Maslowski, 1997, “Improving the Signal to Noise Ratio of Altimetric Measurements in Ice Covered Seas”, (Abstract), EOS Trans. (Suppl.), **78**, F140.

Peacock, N.R., S.W. Laxon, R. Scharoo, W. Maslowski & D.P. Winebrenner, 1998, “Geophysical signature from precise altimetric height measurements in the Arctic Ocean”, Proc. IEEE Geoscience and Remote Sensing Symposium IGARSS’98, Seattle, Washington, IEEE 98CH36174, July 1998, 1964 - 1966

Peltier, W.R., 1988, “Global sea-level and Earth Rotation”, Science, **240**, 895 - 901.

Phalippou, L., 1998, “Feasibility study of a high spatial resolution radar altimeter (HSSRA)” , ESA Contract 12178/96/NL/SB(SC) Final Report.

Picardi, G., R. Sen & S. Sorge, 1998, Extensive Non-Coherent Averaging in Doppler Beam Sharpened Space-Borne Radar Altimeters, Proc. IEEE Geoscience and Remote Sensing Symposium IGARSS’98, Seattle, Washington, IEEE 98CH36174, July 1998, 2643 - 2645.

Piexoto, J.P. & A.H. Oort, 1992, “The Physics of Climate”, American Institute of Physics, New York.

Preller, R.H. , J.E. Walsh & J.A. Maslanik, 1992, “The use of satellite observations in ice cover simulations”, Chapter 22 in Microwave Remote Sensing of Sea Ice (F. Carsey, ed.) AGU Geophysical Monograph **68**, 385 - 404.

Raney, R.K., 1995, “A Delay/Doppler Radar for Ice Sheet Monitoring”, Proc. IEEE Geoscience and Remote Sensing Symposium IGARSS’95, Florence, Italy, IEEE 95CH35770, 862 - 864.

Raney, R.K., 1998, “The Delay/Doppler Radar Altimeter”, IEEE Transactions on Geoscience and Remote Sensing, **36**, 5, 1578 - 1588.

Raney, R.K. & C.J. Leuschen, 2002: LaRA 2002 - Post-Flight Report, JHU/APL SRO-02-13, Laurel, MD, Johns Hopkins University APL, August 2002, 12 pp.

Reeh, N., 1991, “Greenland ice sheet mass balance and sea-level change” in Glaciers, Ice Sheets and sea-level: Effects of a CO_2 induced Climatic Change, National Academy Press, Washington, 155 - 171.

Reeh, N., C. Mayer, H. Miller, H.H. Thomson & A. Weidick, 1999: Present and past climate control on fjord glaciations in Greenland: implications for IRD-deposition in the sea. Geophys. Res. Lett., 26, 1039 - 1042.

Rignot, E.J., 1998, “Fast Recession of a West Antarctic Glacier”, Science, **281**, 549.

Rignot, E.J., 2002, “Mass balance of East Antarctic glaciers and ice shelfes from satellite data”, Annals of Glac., **34**, 217 - 227.

Robin, Q., D.J. Drewry & V.A. Squire, V.A., 1983, “Satellite observations of polar ice fields”, Phil.Trans. R. Soc. London, A **309**, 447.

Rothrock, D.A. & A.S. Thorndike, 1984, “Measuring the Sea Ice Floe Size Distribution”, J. Geophys. Res., **89**, 6477 - 6486.

Rothrock, D.A., Y. Yu & G.A. Maykut, 1999, “Thinning of the Arctic sea-ice cover” Geophys. Research Letters **23**, 3469 - 3472.

Rott, H., P. Skvarca & T. Nagler, 1996, “Rapid Collapse of Northern Larsen Ice Shelf, Antarctica”, Science, **271**, 788 - 792.

Scharroo, R. & P.N.A.M. Visser, 1998, “Precise orbit determination and gravity field improvement for the ERS satellites”, J. Geophys. Res., 103 (C4), 8113 - 8127.

Semtner, A.J., 1996, “A model for thermodynamic growth of sea ice in numerical investigations of climate”, J. Phys. Ocean. **6**, 379 - 389.

Smith, D.M., C. Cooper, D.J. Wingham & S.W. Laxon, 1997, Evaluation of the representation of Arctic sea-ice in the UK Hadley Centre GCM, Ann. Glaciology, **25**, 423 - 428.

Thomas, R.H., T.J.D. Sanderson & K.E. Rose, 1979, “Effects of a climatic warming on the West Antarctic Ice Sheet”, Nature, **227**, 355 - 358.

Thomas, D., S. Martin, D. Rothrock & M. Steele, 1996, “Assimilating satellite concentration data into an Arctic sea ice mass balance model, 1979 - 1985”, J. Geophys. Res., **101**, 20849 -208868.

van der Veen, C.J., 1993, “Interpretation of short-term ice sheet elevation changes inferred from satellite altimetry”, Climatic Change, **23**, 383 - 405.

Varekamp, J.C., E. Thomas & O. Van de Plassche, 1992, “Relative Sea Level Rise and Climate Change over the Past 1500 years”, Terra Nova, 4, 293 - 304.

Vinje, T., N. Nordlund & A. Kvambekk, 1998, “Monitoring ice thickness in the Fram Strait”, J. Geophys. Res., 103, 10437 - 10449.

Wadhams, P., 1990, “Evidence for the thinning of Arctic ice cover north of Greenland”, Nature, 345, 795 - 797.

Wadhams, P., 1995, “Arctic sea ice extent and thickness”, Phil. Trans. Roy. Soc. Lond., 352, 301 - 319.

Wadhams, P., W.B. Tucker III, W.B. Krabill, R.N. Swift, J.C. Comiso & N.R. Davis, 1992, “Relationship Between Sea Ice Freeboard and Draft in the Arctic Basin, and Implications for Ice Thickness monitoring”, J. Geophys. Res., 97, 20325 - 20334

Wahr, J., H. DaZhong & A. Trupin, 1995, “Predictions of vertical uplift caused by changing volumes on a visco-elastic Earth”, Geophys. Res. Lett., 22, 977 - 980.

Wahr, J., C. Bentley & D.J. Wingham, 1998, “What can be learned about Antarctica by combining GRACE and ICESAT (GLAS) satellite data, EOS Trans. (Abs.), G41 F - 06.

Walter, R.A. & M.F. Meier, 1989, “Variability of glacier mass balances in western North America” in Aspects of Climate variability in the Pacific and western Americas, Geophysical Monograph **55**, American Geophysical Union, 365 - 381.

Warrick, R.A., C. Le Provost, M.F. Meier, J. Oerelemans & P.L. Woodworth, 1996, “Changes in Sea Level”, in Climate Change 1995, The Science of Climate Change, Cambridge University Press.

Weaver, A.J. & E.S. Sarachik, 1991, “Evidence for decadal variability in an ocean atmosphere circulation model: An advective mechanism”, Atmosphere-Ocean, **29**, 197-231.

Wingham, D.J., 1995, “Elevation change of the Greenland Ice Sheet”, Phil. Trans. Roy. Soc. Lond., **352**, 342 - 354.

Wingham, D.J., 1995b, “A method for determining the average height of a large ice topogarphic ice sheet from observations of the echo received by a satellite altimeter”, J. Glaciology, **41**, 125 - 141.

Wingham, D.J., 1998, “Short fluctuations in the mass, density and thickness of a dry firn column”, submitted to J. Glaciology.

Wingham, D.J., C.G. Rapley & H.D. Griffiths, 1986, “New techniques in satellite altimeter tracking systems”, in IGARSS’ 86 Symposium Proceedings, Zurich, ESA SP-**245**, 1339 - 1344.

Wingham, D.J., 1997, High Resolution Altimeter Simulation Requirements”, ESA Contract Report UCL-TA-TN-002.

Wingham, D.J., A.J. Ridout, R. Scharroo, R.J. Arthern & C.K. Shum, 1998, “Antarctic Elevation Change 1992 to 1996”, Science, **282**, 456 - 458

WCRP, 1998, “Scientific Concept of the Arctic Climate System Study (ACSYS)”, World Climate Research Program WMO/TD - No. 486.

WCRP, 1998, “CLIVAR Initial Implementation Plan”, World Climate Research Program WMO/TD - No. 869.

Zelli, C., 1998, “High Spatial Resolution Radar Altimeter: Payload Options Definition”, ESA Contract Report, TNO/RAS/0041/ALS Issue 2.

Zwally, H.J., C.L. Parkinson & J.C. Comiso, 1983, “Variation of Anatrctic Sea Ice and Changes in carbon dioxide”, Science, **220**, 1005 - 12.

Zwally, H.J., A.C. Brenner, J.A. Major, R.A. Bindschadler & J.G. Marsh, 1990, “Greenland Ice Sheet: Is it growing or shrinking?”, Science, **248**, 288 - 289.

Zwally, H.J., J.C. Comiso, C.L. Parkinson, D.J. Cavalieri & P. Gloersen, 2002, Variability of Antarctic sea ice 1979–1998, J. Geophys. Res. **107**, 9-1.

CRYOSAT

European Space Agency
Agence spatiale européenne

Contact: ESA Publications Division
c/o ESTEC, PO Box 299, 2200 AG Noordwijk, The Netherlands
Tel. (31) 71 565 3400 - Fax (31) 71 565 5433